Study on the Correlation between Physical Property and Crystal Structure in Layered Perovskite Compounds

(層状ペロブスカイト化合物における物性と結晶構造の関連性に関する研究)

1994

KENJI TODA

Course of Fundamental Science and Technology
Graduate School of Science and Technology
Niigata University

CONTENTS

Chapter 1

General introduction

Perovskite related compounds have many useful applications such as superconductors, dielectrics and catalysts [1 - 6]. It is well known that their physical properties are affected by small deviations from stoichiometry. Since the basic structural component of the perovskite compounds consist of three-dimensional frames of corner shared MO_6 octahedra, the variation of stoichiometry causes large-scale structural rearrangement. The three-dimensional frames are broken along the two-dimensional planes of defects, and shifted, to control the whole stoichiometry of the components. Such a crystallographic shear process results in a long-range ordered two-dimensional structure. Typical examples of such cases are well-known as Ruddlesden-Popper phases, $Sr_{n+1}Ti_nO_{3n+1}$, which involve several kinds of stacking units of the perovskite layer [7]. Ruddlesden-Popper phases are expressed by general formula $A_{n+1}B_nO_{3n+1}$ [= $n(ABO_3) \cdot AO$] for n = 1, 2, 3, and ∞. The conventional perovskite ABO_3 is the end member of the series for $n = \infty$. The A_2BO_4 compound for n = 1 of this series is known as a K_2NiF_4-type compound. The idealized structures of Ruddlesden-Popper phases are shown Fig. 1.1. Since a high temperature superconductor of $(La,Ba)_2CuO_4$ with K_2NiF_4-type structure [8] was discovered in 1986, numerous experimental and theoretical studies have been performed. Also, the relationship between crystal structure and magnetic property in two-dimensional materials have attracted much attention [9 - 11], because their electrical and magnetic properties are governed by the interaction between transition metal and oxygen. The transition metals and oxygen ions

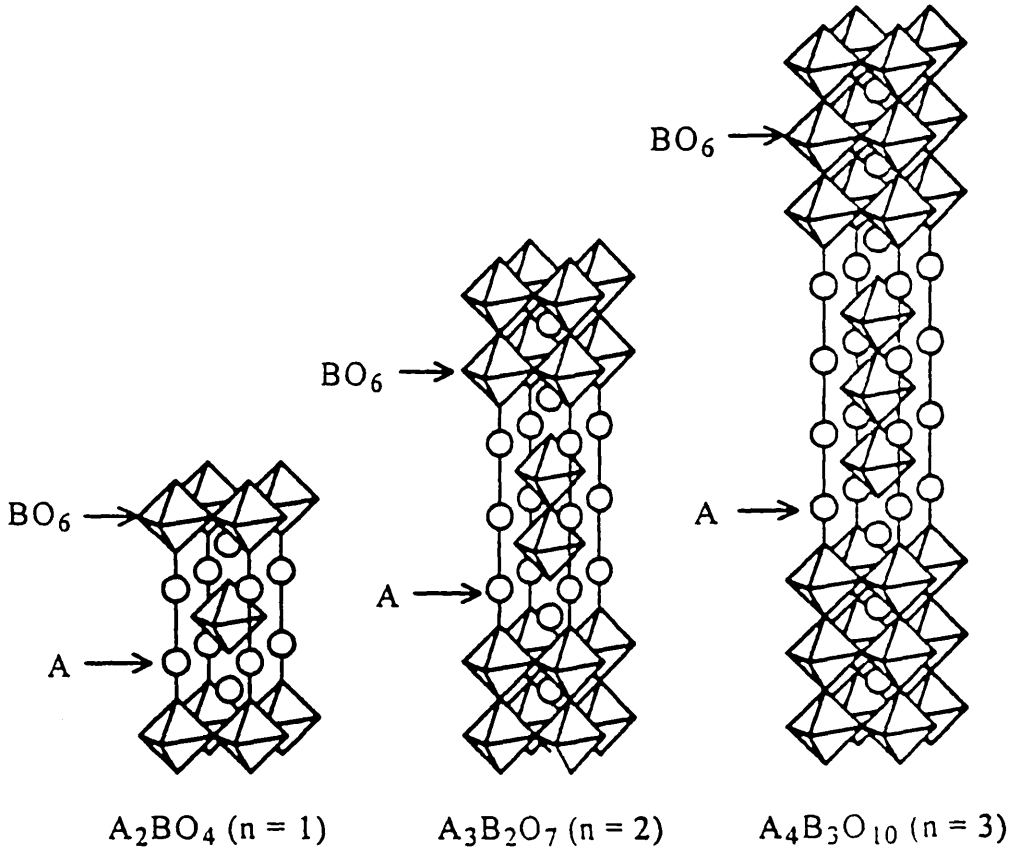

Fig. 1.1 Idealized representations of the structures of Ruddlesden-Popper phases.

in a layered perovskite compound form quasi-two-dimendional plane. Therefore, such a layered perovskite compound is a suitable system to study two-dimensional physical properties coming from the transition metal-oxygen plane. On the other hand, the investigation of physical properties of other cations in the layered perovskite, i.e., A-cations in ABO_3 perovskite, is rather fewer than those of B-cations (transition metals), because A-cations are located on three-dimensional position rather than two-dimensional one in the layered perovskite compound.

In this work, we have paid attention to the layered perovskite compound with ordered A-cations. New layered perovskite compounds with general formula $A_2[Ln_{n-1}Ti_nO_{3n+1}]$, where A = alkali metal and Ln = rare earths, have been recently reported [12, 13]. Since these compounds have two-dimesinal arrays of A-cations, it is of some interest to develop this study focusing on the two-dimensional physical properties of A-cations. We have studied the relationship between the crystal structure and the two-dimensional physical and chemical properties of the ordered layered perovskites. In addition, we tried to prepare some novel layered perovskites with ordered A-cations. This work is composed of six chapters as follows;

In chapter 2, the preparation of a new triple layered perovskite, $Ag_2La_2Ti_3O_{10}$, by an ion-exchange reaction of $K_2La_2Ti_3O_{10}$ with $AgNO_3$ molten salt is described. The effect of the bond character on the ion conductivity behavior in $Ag_2La_2Ti_3O_{10}$ is also discussed.

In chapter 3, the effects of the environment around the conductive ions on the ion conducting behavior in the triple layered perovskite compound, $Na_2La_2Ti_3O_{10}$, are described. The differences of the hydration behavior are also discussed.

In chapter 4, the synthesis of the single layered perovskite compounds, $NaLnTiO_4$ (Ln = La, Eu, Gd, Y, and Lu), are described. By using two parameters of c/a ratio and tolerance factor t, the change of symmetry of crystal structure was explained. The lowering of the symmetry is discussed in terms of the mismatch between TiO_2 and LnO_2 layers.

In chapter 5, the preparations of the new single layered perovskites, $AgLnTiO_4$ and $LiLnTiO_4$ (Ln = La and Eu), are described. The difference in the crystal structure between both compounds is discussed in terms of the ionic radius of the interlayer A-cations.

In chapter 6, the critical dopant concentration for photoluminescence of $NaGdTiO_4$ and $Na_2Gd_2Ti_3O_{10}$ doped by Eu^{3+} is discussed in terms of their two-dimensional crystal structures. We pointed out that the concentration quenching found in these compounds can be explained by means of a percolation model.

The contents of this thesis are composed of the following papers.

1. M. Sato, K. Toda, J. Watanabe and K.Uematsu, *Nippon Kagaku Kaishi*, 640 (1993)

2. K. Toda, Y. Kameo, M. Ohta and M. Sato, *J. Ceram. Soc. Japan*, 102, 737 (1994)

3. K. Toda, Y. Kameo, M. Ohta and M. Sato, *J. Alloys Comp.*, in press

Chapter 2

Structure Determination and Ion Conductivity of a Layered Perovskite Compounds, $M_2La_2Ti_3O_{10}$ (M =K and Ag).

2.1 Introduction

Layered perovskite compounds have been investigated extensively in the literature because they exhibit a variety of structural and electric properties. However, ionic conduction, especially cationic conduction, has been scarcely studied for these type oxides. Recently, ion-exchangeable layered perovskites made up of NbO_6 or TiO_6 octahedra have gained interest, because of not only their excellent ion-exchange ability but also their intercalation reactions [12 - 21] and photocatalytic reactions [22]. The synthesis of $M_2La_2Ti_3O_{10}$ (M = Li, Na, K) has been reported for the first time by Vallino [23]. Recently ion-exchange reactions of $M_2Ln_2Ti_3O_{10}$ (M = Na, K, Rb; Ln = rare earth ions) have been found independently by Gondrand and Joubert [12] and Gopalakrishnan and Bhat [13]. However, the crystal structure of $M_2Ln_2Ti_3O_{10}$ remains unknown although prototype structure models are presumed on the basis of lattice constants and on the indexing of the powder X-ray diffraction (XRD) patterns.

In the course of the study for these compounds, we have found that the potassium ions in the parent compound, $K_2La_2Ti_3O_{10}$, are readily exchanged with silver ions in $AgNO_3$ molten salt to give a new layered perovskite compound, $Ag_2La_2Ti_3O_{10}$. It is well known that Ag^+ ion can be a

mobile cation in various ionic conductors. Therefore, ionic conductive behavior for $Ag_2La_2Ti_3O_{10}$ would be quite interest.

In this chapter, the structure and ionic conductivity of $Ag_2La_2Ti_3O_{10}$ are investigated and are compared with those of the niobate compound $AgLaNb_2O_7$ [18]. On the basis of the comparison between titanate and niobate compounds, we have discussed the mechanism of the ionic conductive behavior in the layered perovskite compounds.

2.2 Experimental

$K_2La_2Ti_3O_{10}$ was prepared by a conventional solid-state reaction. The starting materials were K_2CO_3, La_2O_3 and TiO_2. An excess amount of K_2CO_3 (30mol%) was added to compensate for loss due to the evaporation of potassium component. The reactants were ground, pelletized and then fired in an open alumina crucible. The mixture was fired for 6h at 550℃, further heated for another 6h at 1000℃ in air. After the reaction, the product was washed with distilled water and dried for 24h at 100℃. The ion-exchange reaction was done by adding the ground $K_2La_2Ti_3O_{10}$ powder to a molten salt of $AgNO_3$ at 250℃ for 72h. After the reaction, the precipitate of $Ag_2La_2Ti_3O_{10}$ was collected, washed with distilled water again and dried for 24h at 100℃.

Analysis of the ion-exchange compound for residual alkali metal was carried out by Electron Probe Micro-Analysis (EPMA). Thermogravimetric analysis (TGA) and differential thermal analysis (DTA) were carried out using a Mac Science thermal analyzer system 001 at a heating rate of 5℃ min^{-1} in air. Powder XRD patterns were recorded on a Rigaku RAD-rA diffractometer, using Cu-K α radiation which was monochromatized by a curved crystal of graphite. The data were collected in a step-scanning mode in the 2θ range of 5 - 100° with a step width of 0.02° and a step time of 4s. Indexing of the powder XRD patterns obtained was examined with the aid of the computer program CELL [24]. Data analysis was carried out by the Rietveld method, using the RIETAN profile refinement program [25] on an ACOS2010 computer at Niigata University. An extended pseudo-Voigt function was chosen to generate the line shape of the diffraction peaks. A

modified Marquardt algorithm was used in nonlinear least-squares procedures. The reflection peak observed at low 2θ region in the powder diffraction pattern was found to deviate greatly from the calculated peak profile due to an asymmetric effect of peak shape. Therefore, this reflection peak was eliminated from the Rietveld refinement.

The Ag^+ ion conductivity and electronic conductivity of $Ag_2La_2Ti_3O_{10}$ were measured by two-probe alternating current (AC) and direct current (DC) technique. The AC conductivity was determined using the complex impedance diagrams of the data obtained between 40Hz and 100kHz, using a HIOKI 3520Hi Tester. Powder samples were compressed in a pellet at 400MPa. Silver past was used as the electrode. AgI was used as an ionically blocking electrode for the measurement of DC conductivity. The pure ion conductivity was determined by measuring the voltage between both opposite faces of a cell (Pt, Ag | AgI | sample | Ag, Pt) using a digital-multitester (ADVANTEST TR2114).

2.3 Results and Discussion

From the powder XRD measurement of $K_2La_2Ti_3O_{10}$, this compound was found to intercalate water molecules in the interlayer space. Figure 2.1 shows the thermogravimetric curve of $K_2La_2Ti_3O_{10} \cdot xH_2O$ fully hydrated by an atmosphere with 100% humidity at room temperature. The weight losses from room temperature to 100℃ and from 100 to 200℃ correspond to the loss of 0.27mol of absorbed surface water molecules and 1.97mol of interlayer hydration water molecules, respectively. Therefore, the value of x can be estimated about 2. On the other hand, the silver ion-exchange compound is not hygroscopic. The EPMA result indicates that both Ag^+ and K^+ in the ion-exchange compound are present in molar ratio of Ag : K = 1.91 : 0.13. The ion-exchange reaction was almost complete.

The synthesis of $K_2La_2Ti_3O_{10}$ has been reported by Gopalakrishnan and Bhat [13]. However, the crystal structure of $K_2La_2Ti_3O_{10}$ remains unknown although prototype structure models are presumed on the basis of lattice constants and on the indexing of the powder XRD patterns. In this study, the crystal structures of three compounds, $K_2La_2Ti_3O_{10} \cdot 2H_2O$, $K_2La_2Ti_3O_{10}$ and $Ag_2La_2Ti_3O_{10}$, were determined by the Rietveld analysis. Since anhydrate $K_2La_2Ti_3O_{10}$ can easily intercalate water molecules in ambient air, the measurement of powder XRD was carried out at 200℃, using a high temperature furnace attachment. All the reflections obtained for these compounds could be assigned as a tetragonal symmetry. It was found to be no reflection condition for $K_2La_2Ti_3O_{10} \cdot 2H_2O$, leading to eight possible space groups with P-type lattice (P4, $P\bar{4}$, P4/m, P422. P4mm, $P\bar{4}2m$, $P\bar{4}m2$ and P4/mmm). The indexing for $K_2La_2Ti_3O_{10}$ and $Ag_2La_2Ti_3O_{10}$ was

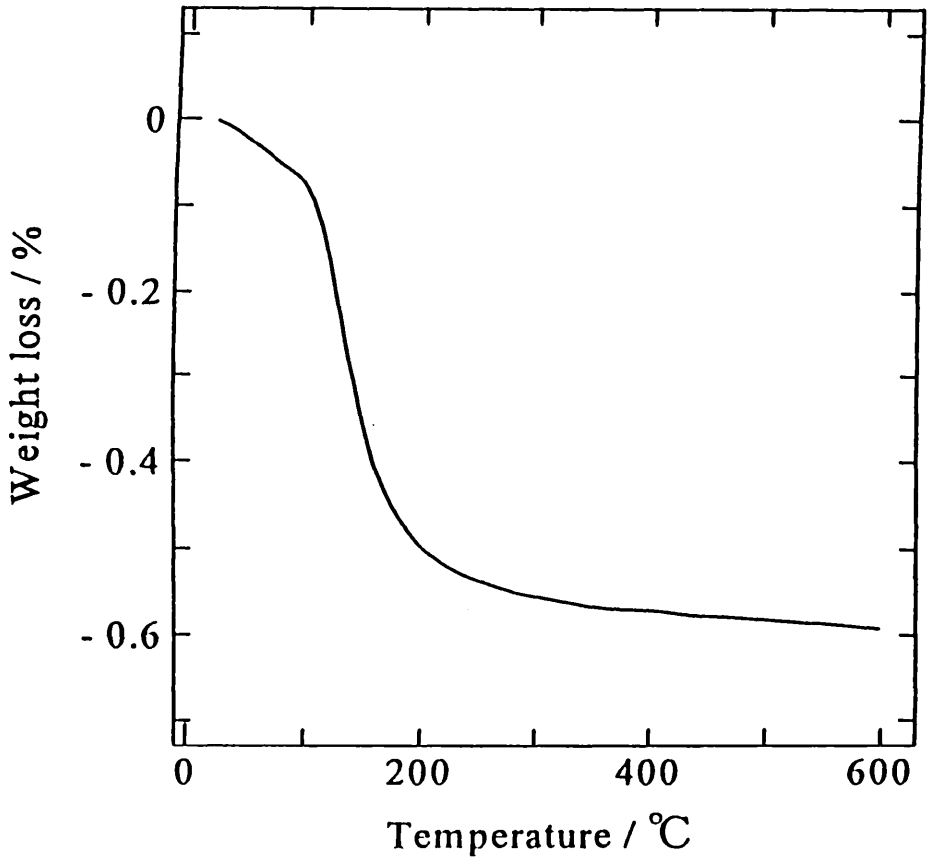

Fig. 2.1 Thermogravimetric curve of $K_2La_2Ti_3O_{10} \cdot xH_2O$ fully hydrated by an atmosphere with 100% humidity at 25℃

also examined. The reflection condition found for both compounds was h + k + l = 2n for hkl reflections, giving eight possible space groups with I-type lattice (I4, $I\bar{4}$, I4/m, I422, I4mm, $I\bar{4}m2$, $I\bar{4}2m$ and I4/mmm). An initial structural model for $K_2La_2Ti_3O_{10} \cdot 2H_2O$ was adopted on the basis of assumption that the main lattice of $La_2Ti_3O_{10}$ layer constructs a triple perovskite layer analogous to $CsCa_2Nb_3O_{10}$ which has triple perovskite layers without displacement of each layer as reported by Dion et al. [14]. On the other hand, since $K_2La_2Ti_3O_{10}$ and $Ag_2La_2Ti_3O_{10}$ have a body centered Bravais lattice, an initial structural model was constructed by taking account the displacement of each perovskite layer along the c-axis. The Rietveld refinement was carried out for all space groups given by the CELL results in the first refinement stage. The most reliable solutions with physically meaningful crystallographic parameters was finally achieved when adopting P4/mmm space group for $K_2La_2Ti_3O_{10} \cdot 2H_2O$ and I4/mmm space group for $K_2La_2Ti_3O_{10}$ and $Ag_2La_2Ti_3O_{10}$. The site occupancy of water molecule (only oxygen atom was assigned) in $K_2La_2Ti_3O_{10} \cdot 2H_2O$ was also refined in the final refinement stage. The crystallographic data and the positional parameters are listed in Table 2.1. A typical result of the pattern fitting is shown in Fig. 2.2 for $K_2La_2Ti_3O_{10} \cdot 2H_2O$. The selected interatomic distances and angles are listed in Tables 2.2 - 2.4. The crystal structures of three compounds refined are shown in Figs. 2.3 and 2.4. The structural features of $K_2La_2Ti_3O_{10} \cdot 2H_2O$ is substantially the same as that reported by Gopalakrishnan and Bhat [13]. However, the composition and position of water molecules are different from their model. Water molecules are statistically distributed in a 4m (x, 0, 1/2) site with 40% occupancy, giving 1.6mol water molecules for formula unit. Results of TG and the Rietveld

Table 2.1 Crystallographic data and positional parameters of $K_2La_2Ti_3O_{10} \cdot 2H_2O$, $K_2La_2Ti_3O_{10}$ and $Ag_2La_2Ti_3O_{10}$

	Atom	Site[a]	g[b]	x	y	z	B / nm²
$K_2La_2Ti_3O_{10} \cdot 2H_2O$	K	2h	1.0	0.5	0.5	0.3797(14)	0.025(5)
P4/mmm (No. 123)	La	2h	1.0	0.5	0.5	0.1285(3)	0.001(1)
a = 0.38585(1)nm	Ti(1)	1a	1.0	0.0	0.0	0.0	0.001
c = 1.6814(1)nm	Ti(2)	2g	1.0	0.0	0.0	0.2510(7)	0.001
R_{wp} = 13.69%	O(1)	2f	1.0	0.0	0.5	0.0	0.033(17)
R_p = 10.60%	O(2)	2g	1.0	0.0	0.0	0.1142(24)	0.002(11)
R_I = 4.84%	O(3)	4i	1.0	0.0	0.5	0.2271(17)	0.002(8)
R_F = 2.42%	O(4)	2g	1.0	0.0	0.0	0.3521(20)	0.004(12)
	Ow[c]	4m	0.40(3)	0.25(2)	0.0	0.5	0.081(59)
$K_2La_2Ti_3O_{10}$	K	4e	1.0	0.0	0.0	0.2923(4)	0.018(4)
I4/mmm (No. 139)	La	4e	1.0	0.0	0.0	0.4276(1)	0.018(1)
a = 1.25436(2)nm	Ti(1)	2a	1.0	0.0	0.0	0.0	0.015(4)
c = 0.53281(4)nm	Ti(2)	4e	1.0	0.0	0.0	0.1413(3)	0.013(3)
R_{wp} = 10.19%	O(1)	4c	1.0	0.0	0.5	0.0	0.060(15)
R_p = 7.71%	O(2)	4e	1.0	0.0	0.0	0.0643(15)	0.049(11)
R_I = 2.73%	O(3)	8g	1.0	0.0	0.5	0.1295(8)	0.025(7)
R_F = 1.46%	O(4)	4e	1.0	0.0	0.0	0.1989(11)	0.022(10)
$Ag_2La_2Ti_3O_{10}$	Ag	4e	1.0	0.0	0.0	0.2872(4)	0.017(2)
I4/mmm (No. 139)	La	4e	1.0	0.0	0.0	0.4249(2)	0.001(1)
a = 1.25436(2)nm	Ti(1)	2a	1.0	0.0	0.0	0.0	0.001(7)
c = 0.53281(4)nm	Ti(2)	4e	1.0	0.0	0.0	0.1483(6)	0.002(5)
R_{wp} = 12.64%	O(1)	4c	1.0	0.0	0.5	0.0	0.053(28)
R_p = 9.14%	O(2)	4e	1.0	0.0	0.0	0.0653(23)	0.007(14)
R_I = 3.73%	O(3)	8g	1.0	0.0	0.5	0.1344(12)	0.016(13)
R_F = 2.76%	O(4)	4e	1.0	0.0	0.0	0.2087(20)	0.001(15)

a) Multiplicity and Wyckoff notation.
b) Occupancy.
c) Oxygen atom of water molecule.

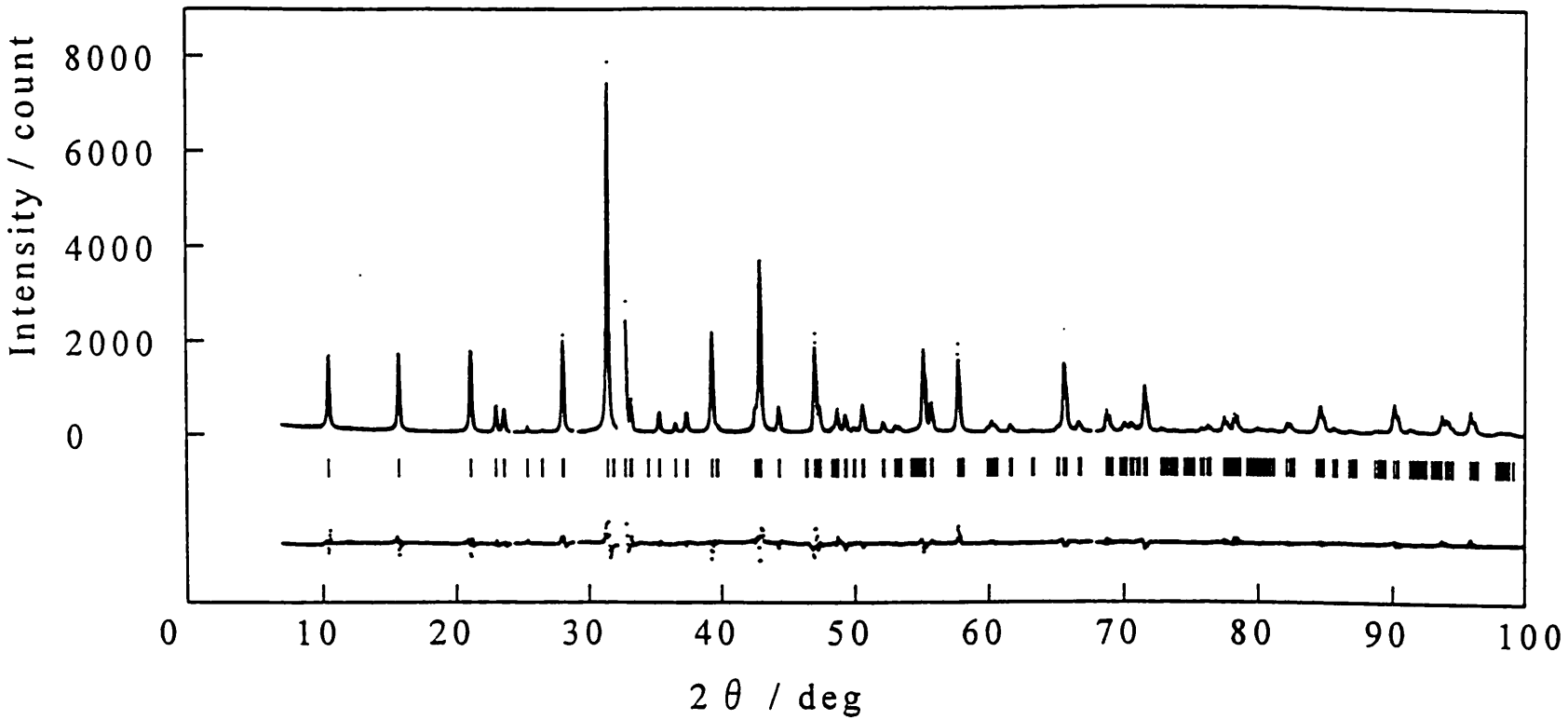

Fig. 2.2 Powder X-ray diffraction pattern fitting for $K_2La_2Ti_3O_{10} \cdot 2H_2O$. The calculated and observed patterns are shown on the top solid line and the dots, respectively. The vertical marks in the middle show positions calculated Bragg reflections. The trace on the bottom is a plot of the difference between calculated and observed intensities.

Table 2.2 Bond distances (nm) and angles (°) of $K_2La_2Ti_3O_{10} \cdot 2H_2O$

Distance		Angle	
K - O(4)	0.2767(4)x4	O(2) - Ti(2) - O(3)	78.2(7)x4
K - Ow	0.281(22)x4		
La - O(1)	0.2897(4)x4		
La - O(2)	0.2739(3)x4		
La - O(3)	0.2542(18)x4		
Ti(1) - O(1)	0.1929(1)x4		
Ti(1) - O(2)	0.1920(41)x2		
Ti(2) - O(2)	0.2300(42)		
Ti(2) - O(3)	0.1970(5)x4		
Ti(2) - O(4)	0.1701(35)	Symmetry code	
O(1) - O(1)$^{i)}$	0.2728(1)x4		
O(1) - O(2)	0.2722(29)x4	None	x, y, z
O(2) - O(3)	0.2706(33)x4	i)	-y, x, z
O(3) - O(3)$^{ii)}$	0.2728(1)x4	ii)	-x, -y, z
O(3) - O(4)	0.2854(32)x4		
Ow - O(4)	0.2673(68)		
Ow - Ow$^{ii)}$	0.196(34)		
Ow - Ow$^{i)}$	0.139(24)		

Table 2.3 Bond distances (nm) and angles (°) of $K_2La_2Ti_3O_{10}$.

Distance		Angle	
K - O(4)	0.2787(36)	O(2) - Ti(2) - O(3)	79.7(7)x4
K - O(4)$^{i)}$	0.2753(3)x4	O(4) - K - O(4)$^{i)}$	95.3(7)x4
K - O(3)$^{i)}$	0.3030(21)x4		
La - O(1)$^{i)}$	0.2901(4)x4		
La - O(2)$^{i)}$	0.2751(4)x4		
La - O(3)$^{i)}$	0.2580(17)x4		
Ti(1) - O(1)	0.1938(1)x4		
Ti(1) - O(2)	0.1918(47)x2		
Ti(2) - O(2)	0.2296(48)		
Ti(2) - O(3)	0.1970(4)x4		
Ti(2) - O(4)	0.1719(34)	Symmetry code	
O(1) - O(1)$^{ii)}$	0.2741(1)x4		
O(1) - O(2)	0.2727(33)x4	None	x, y, z
O(2) - O(3)	0.2745(36)x4	i)	1/2-x, 1/2-y, 1/2-z
O(3) - O(3)$^{ii)}$	0.2741(1)x4	ii)	-y, x, z
O(3) - O(4)	0.2836(30)x4		

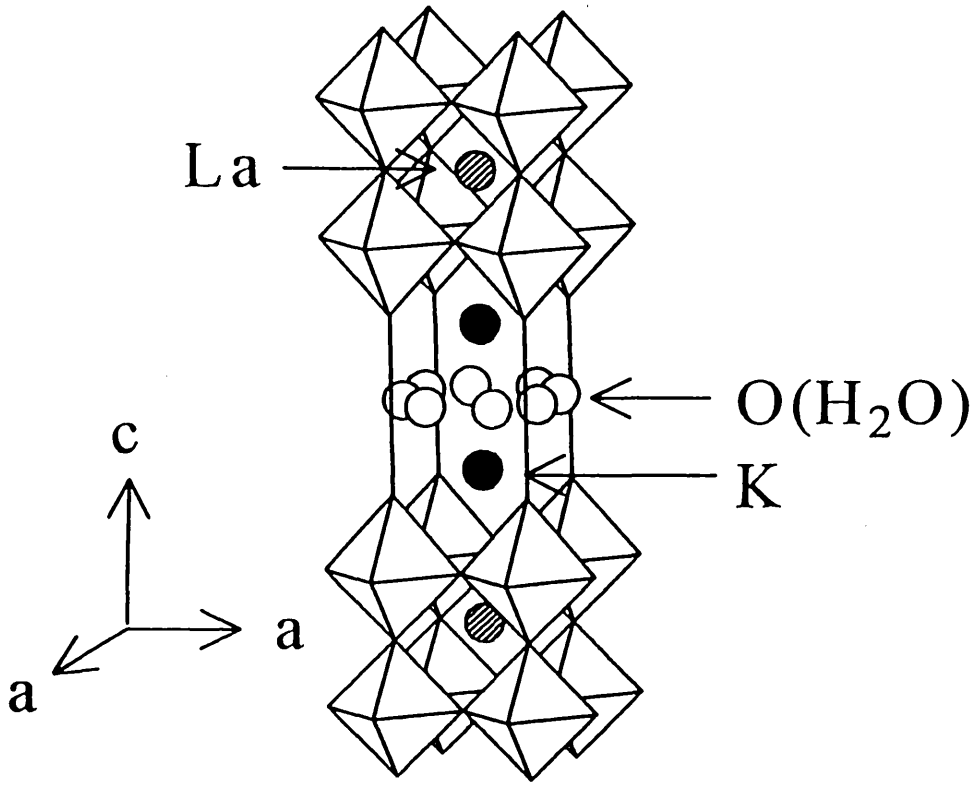

Fig. 2.3 Crystal structure of $K_2La_2Ti_3O_{10} \cdot 2H_2O$. The octahedra are TiO_6 units. The shaded circle within the layer are La atoms. The filled and open circles represent potassium atoms and oxygen atoms of water molecules, respectively.

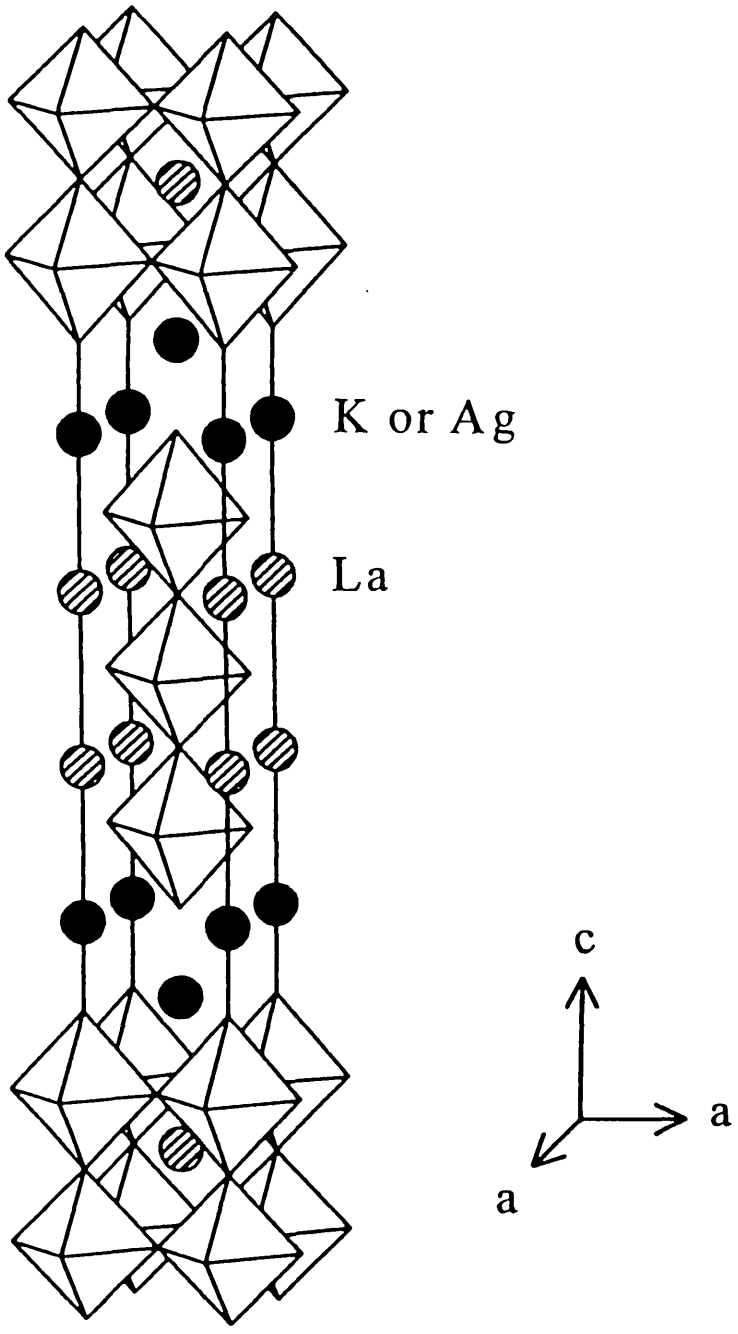

Fig. 2.4 Crystal structure of $K_2La_2Ti_3O_{10}$ and $Ag_2La_2Ti_3O_{10}$.

Table 2.4 Bond distances (nm) and angles (°) of $Ag_2La_2Ti_3O_{10}$.

Distance		Angle	
Ag - O(4)	0.2268(57)	O(2) - Ti(2) - O(3)	78.1(11)x4
Ag - O(4)[i)]	0.2707(2)x4	O(4) - Ag - O(4)[i)]	92.4(13)x4
Ag - O(3)[i)]	0.2962(30)x4		
La - O(1)[i)]	0.2891(5)x4		
La - O(2)[i)]	0.2719(7)x4		
La - O(3)[i)]	0.2568(26)x4		
Ti(1) - O(1)	0.1912(1)x4		
Ti(1) - O(2)	0.1886(67)x2		
Ti(2) - O(2)	0.2397(67)		
Ti(2) - O(3)	0.1954(8)x4		
Ti(2) - O(4)	0.1744(62)	Symmetry code	
O(1) - O(1)[ii)]	0.2704(1)x4		
O(1) - O(2)	0.2686(47)x4	None	x, y, z
O(2) - O(3)	0.2764(55)x4	i)	1/2-x, 1/2-y, 1/2-z
O(3) - O(3)[ii)]	0.2704(1)x4	ii)	-y, x, z
O(3) - O(4)	0.2874(47)x4		

refinement can be taken to be consistent with above results. Gopalakrishnan and Bhat claimed that water molecules are located in a 1b (0, 0, 1/2) site with 1mol for formula unit. The Rietveld analysis on basis of their model gave no reasonable solution with physically meaningful structural parameters. However, the values of isotropic thermal parameters are highly scattered in our model. In particular, the value for Ow (oxygen atom of water molecules) is considerably large, and some of values for other sites must be fixed to a positive value because they converge to negative values without fixing. This may be due to compositional and positional disorders of water molecules. It is difficult to obtain accurate information of water molecules (oxygen atom) from powder XRD pattern analysis. Another approach, for example, neutron diffraction pattern analysis, is necessary to give a precise structural description of the water molecules. The structures of anhydrous $K_2La_2Ti_3O_{10}$ and $Ag_2La_2Ti_3O_{10}$ were well analogous to that of the Ruddlesden-Popper phase with the tetragonal crystal system. The adjacent triple perovskite sheets, $La_2Ti_3O_{10}$, are stacked with a displacement by 1/2 along the (110) direction. Contrary to the niobium compounds, anhydrous $K_2La_2Ti_3O_{10}$ and $Ag_2La_2Ti_3O_{10}$ have almost the same crystal structure. In niobate oxides with a layered perovskite structure, the relative arrangement of the adjacent perovskite sheets is dependent of its ionic size existing in the interlayer. $KLaNb_2O_7$ [21] forms a base-centered lattice wherein potassium ions have trigonal prismatic coordination, while $AgLaNb_2O_7$ [18] takes a body-centered lattice wherein silver ions have tetrahedral coordinations.

Figure 2.5 shows the environment of titanium atoms in $Ag_2La_2Ti_3O_{10}$. The TiO_6 octahedron located on the inside of the perovskite layers is close

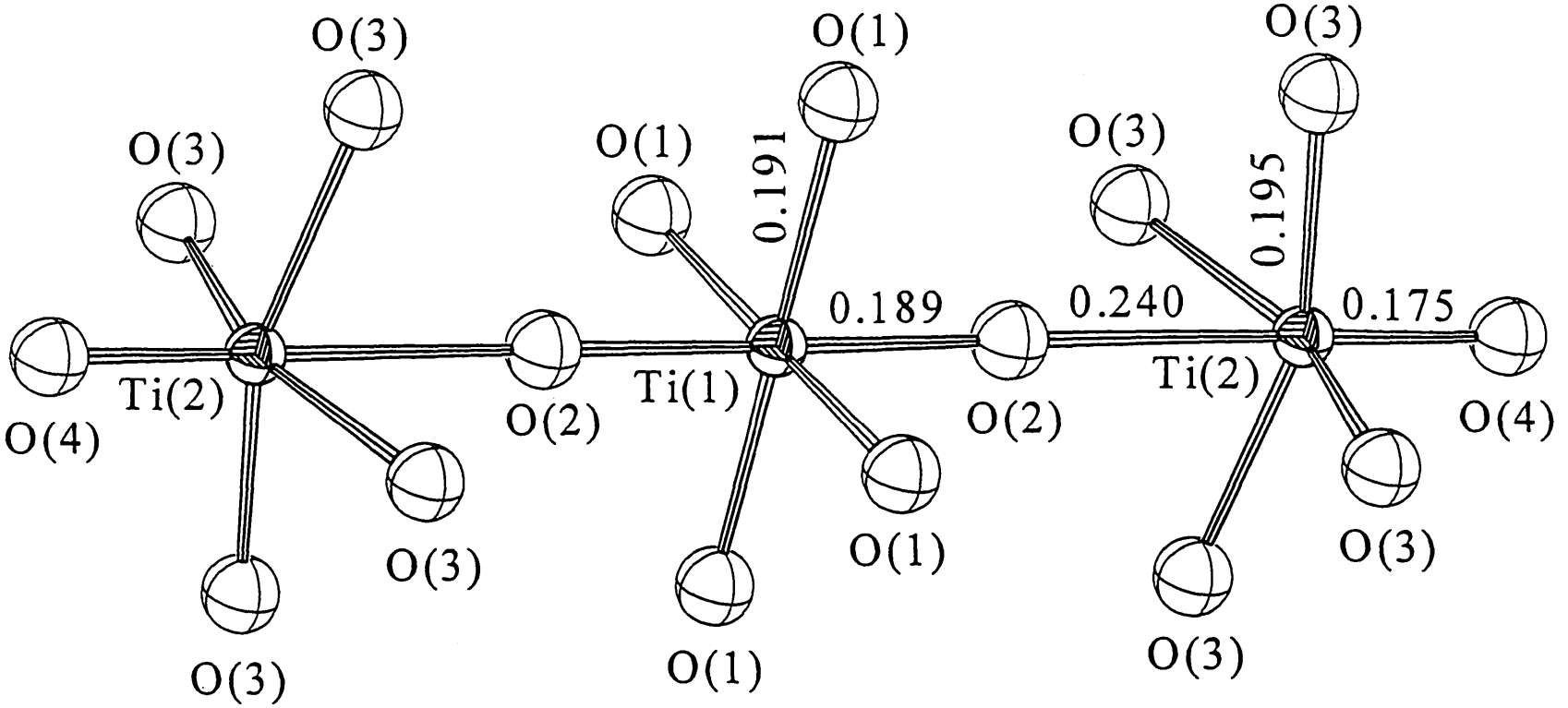

Fig. 2.5 Linkage of TiO_6 octahedra in $Ag_2La_2Ti_3O_{10}$.

to an ideal octahedron, while those located on the outside of the layer are fairly distorted. The Ti - O bonds of the latter octahedra in these compounds are classified into three types, i.e., a very shortened bond (Ti(2) - O(4)) toward the interlayer space, four normal bonds (Ti(2) - O(3)) linked with an equatorial oxygen atom and a long bond (Ti(2) - O(2)) toward the inside of the layer. These bond characters are similar to those of $KLaNb_2O_7$ [21] and $AgLaNb_2O_7$ [18]. Figure 2.6 shows the environment around Ag ion located between the two perovskite layers. The potassium and silver ions in these compounds occupy nine-fold sites with a distorted rock-salt-type coordination between the two perovskite layers. Although the anhydrous $K_2La_2Ti_3O_{10}$ and $Ag_2La_2Ti_3O_{10}$ had almost the same crystal structure, a drastic difference in the bond character of M-O (M = K, Ag) was observed between the two compounds. The Ag - O bonds of this coordination are classified into two types, i.e., shortened bonds (0.2268nm) toward the c-axis direction, four long bonds (0.2707nm) toward inside of the layer. The shortened bond is smaller than the sum of Shannon's ionic radius [26]. This bond distance is similar to those observed for silver atoms have a covalent bond character in oxide [27, 28]. Therefore, it seems that there is relatively strong covalent character for the Ag - O bond along the direction of c axis. While, two K - O bond distances (0.2787, 0.2753nm) are comparable with the sum of Shannon's ionic radius (0.273nm), indicating completely ionic character. Such a covalent bond character in $Ag_2La_2Ti_3O_{10}$ was reflected to the conductivity behavior shown latter.

A typical impedance plot for $Ag_2La_2Ti_3O_{10}$ at 106℃ are shown in Fig. 2.7. In all cases, the impedance plot are semicircles, indicating almost absence of electrode surface effects. Accordingly, the bulk conductivity is

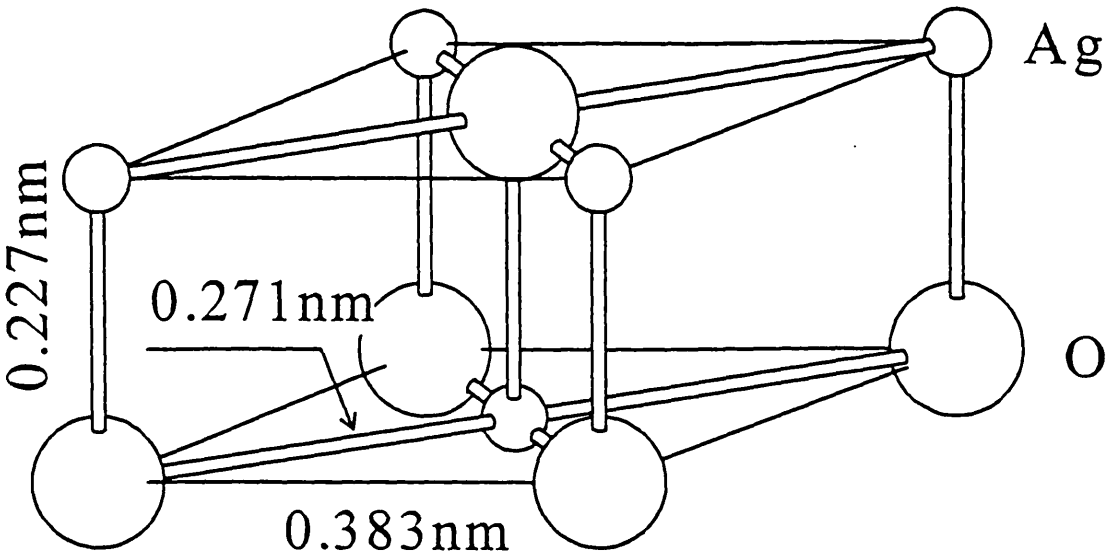

Fig. 2.6 Environment around Ag ion located between two perovskite layers.

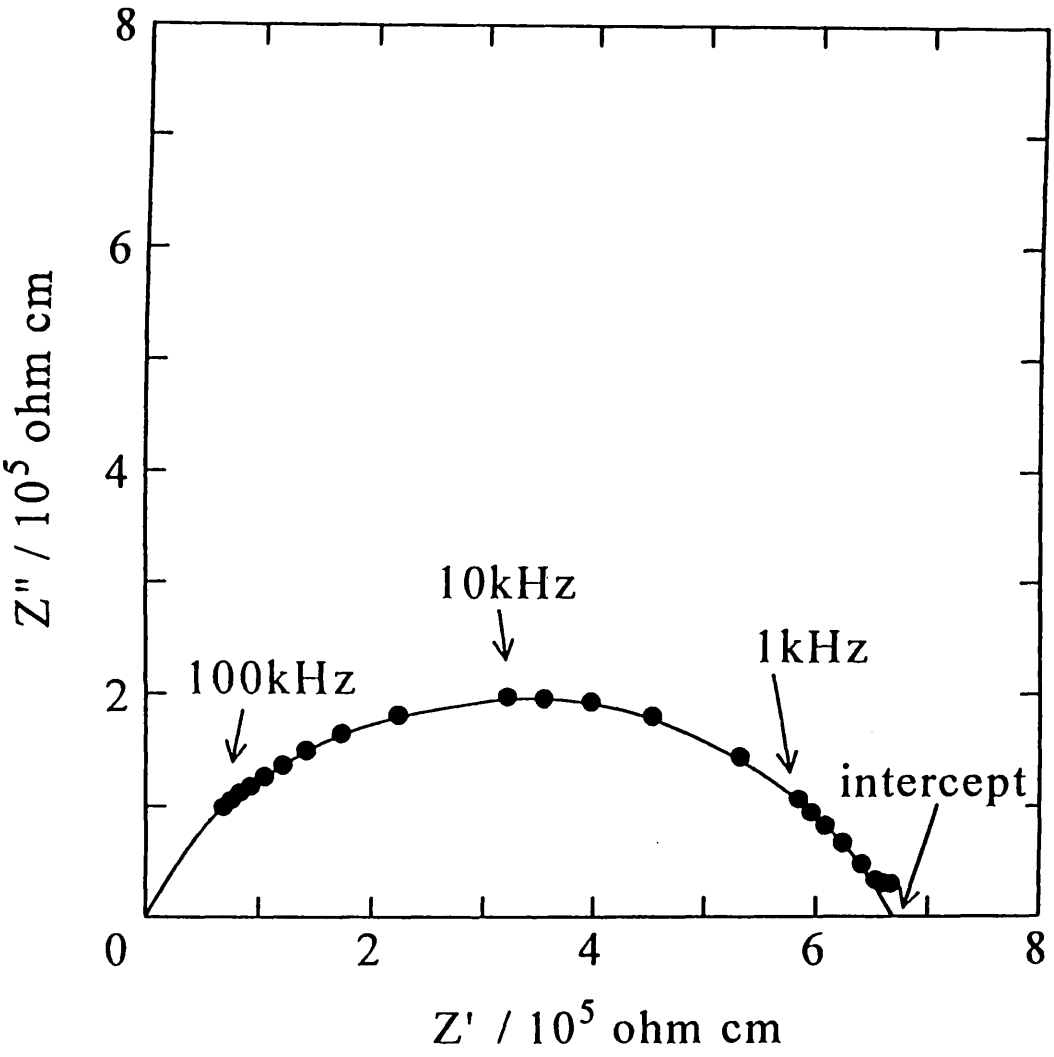

Fig. 2.7 Impedance diagram obtained at 106℃ for $Ag_2La_2Ti_3O_{10}$. The solid line was calculated by a nonlinear least squares method. Z' and Z'' mean the real and imaginary components of impedance, respectively.

determined from the low frequency intercept of the semicircle. Figure 2.8 shows the temperature dependence of AC and DC conductivity for $Ag_2La_2Ti_3O_{10}$. AC conductivity is in almost agreement with DC conductivity below 200℃. It is shown that almost pure ion conduction of silver was observed at this temperature range. AC conductivity is higher than DC conductivity above 200℃. Mixed conduction was observed over this temperature with the silver ion transport number t_{ion} = 0.54 at 300℃ and t_{ion} = 0.51 at 400℃. It is apparent that the this mixed conduction is due to relatively strong covalent character for the Ag - O bond along the direction of c axis as mentioned above. In addition, the activation energy of DC conductivity above 200℃ decreases with increasing temperature. The calculated activation energies above and below 200℃ were 42.8kJmol^{-1} and 55.6kJmol^{-1}, respectively. This phenomenon may be attributed to the change of band structure because DTA shows no structural phase transition with rearrangement of atoms at this temperature. The value of ionic conductivity for $Ag_2La_2Ti_3O_{10}$ are rather smaller than those for so-called fast ion conductors [29, 30]. However, pure ion conduction found for $Ag_2La_2Ti_3O_{10}$ in low temperature region is extremely rare in the normal oxide because of silver atoms tend to have a covalent bond character in oxides. It is interesting to compare the ionic conductivity of $Ag_2La_2Ti_3O_{10}$ with that of niobate compound [18]. The silver ions of $Ag_2La_2Ti_3O_{10}$ are situated in a rigid rock-salt-type coordination with 100% occupancy. On the other hand, silver ions in $AgLaNb_2O_7$ are located in a tetrahedral coordination with 50% occupancy. Consequently, the value of ionic conductivity of $Ag_2La_2Ti_3O_{10}$ is approximately 10 times less than that of niobate compound, $AgLaNb_2O_7$ [18]. However, structural phase transition in $AgLaNb_2O_7$ at about 300℃ leads to

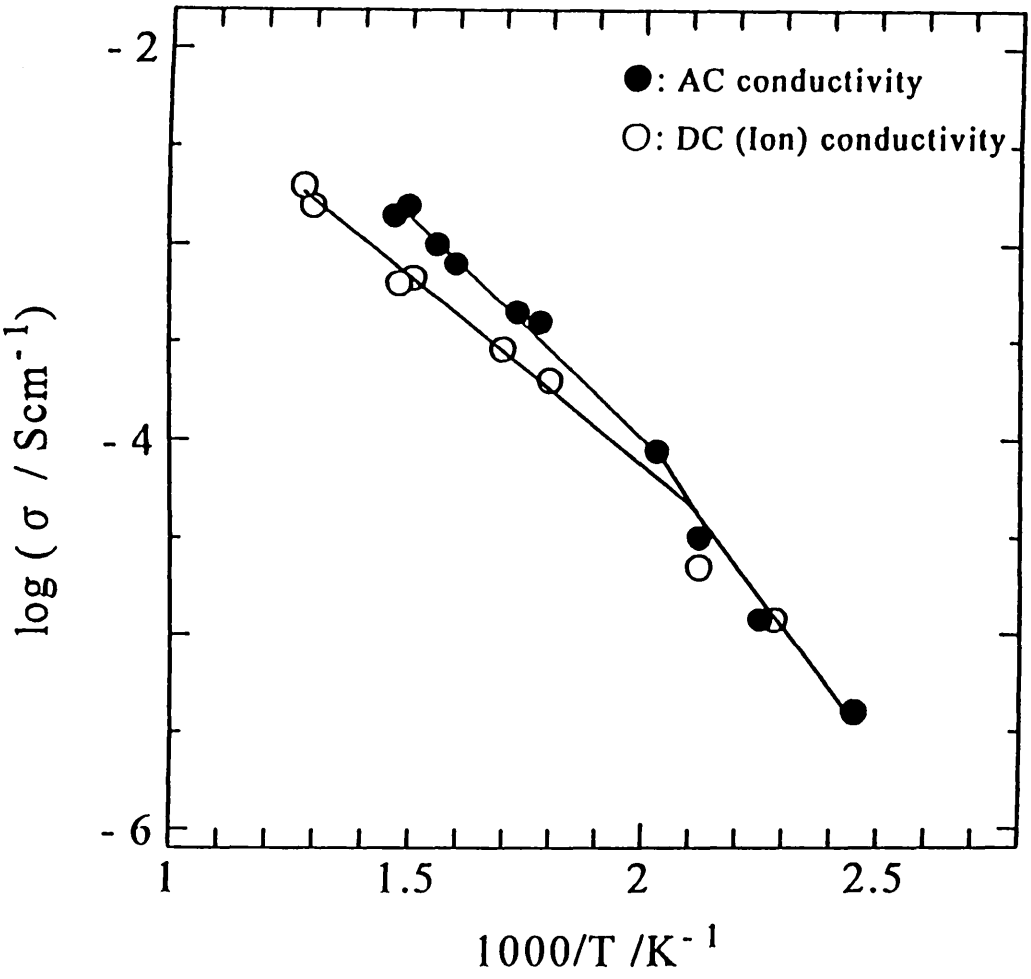

Fig. 2.8 Temperature dependence of conductivity for $Ag_2La_2Ti_3O_{10}$.

an abrupt decrease in the conductivity. In $Ag_2La_2Ti_3O_{10}$, such a decrease of conductivity do not observed because structural phase transition is absent.

2.4 Summary

A layered perovskite compound, $Ag_2La_2Ti_3O_{10}$, was newly synthesized by an ion exchange reaction of $K_2La_2Ti_3O_{10}$ with a $AgNO_3$ molten salt. The crystal structures of the parent compound $K_2La_2Ti_3O_{10} \cdot xH_2O$ and the ion-exchanged compound $Ag_2La_2Ti_3O_{10}$ were determined by Rietveld analysis. All the structures were analogous to that of Ruddlesden-Popper phase with a tetragonal crystal system. Although the anhydrous $K_2La_2Ti_3O_{10}$ and $Ag_2La_2Ti_3O_{10}$ compound have almost the same crystal structure, a drastic difference in the bond character of M-O (M = K, Ag) was observed between the two compounds, i.e., completely ionic character for the K-O bond and relatively strong covalent character for the Ag-O bond along the direction of the c axis. Such a covalent bond character in $Ag_2La_2Ti_3O_{10}$ was reflected to the conductivity behavior. An almost pure ion conduction of silver was observed at the temperatures below 200℃, while the mixed conduction with silver ion transport number of 0.5 was observed over this temperature.

Chapter 3

Crystal Structure and Ionic Conductivity of a Layered Perovskites, $Na_2La_2Ti_3O_{10}$.

3.1 Introduction

Recently, a great interest has developed in ion-exchangeable layered perovskites made up of NbO_6 or TiO_6 octahedra, not only because of excellent ability of ion-exchange reaction but also their intercalation reactions [12 - 21] and photocatalytic reactions [22]. Sodium compound, $Na_2La_2Ti_3O_{10}$, is one of the member of Ruddlesden-Popper type ion-exchangeable layered perovskite. This compound can be directly obtained by a conventional solid state reaction. Therefore, we expected that $Na_2La_2Ti_3O_{10}$ have applicability as a solid electrodes. However, the crystal structure of $Na_2La_2Ti_3O_{10}$ remains unknown although prototype structure models are presumed on the basis of lattice constants and on the indexing of the powder XRD patterns. Though many of the ion-exchangeable compounds containing sodium ions, for example, Na- β -alumina, exhibit high ionic conductivity, there are few studies on ionic conductivity of interlayer ions for layered perovskites consisting of TiO_6 octahedra.

In chapter 2, we have clarified the silver ionic conductive properties of a silver-exchanged compound $Ag_2La_2Ti_3O_{10}$, which crystallizes into a Ruddlesden-Popper structure and exhibits a relatively strong covalent character for the Ag-O bond along the direction perpendicular to the perovskite layer [17]. It shows mixed conduction with silver ions and

electrons above 200℃. On the other hand, the main structure of $AgLaNb_2O_7$ which shows almost pure ionic conduction is also analogous to that of the Ruddlesden-Popper phase but the environment around the interlayer ions in this compound is somewhat different, i.e., silver ions are located on the nearly tetrahedral site with 50% occupancy in the interlayer [18]. These structural differences between titanates and niobates are thought to be reflected by their conductive behaviors. This is because the TiO_6 and NbO_6 octahedra exhibit the different interactions between the perovskite sheets and the interlayer ions due to the different oxidation states of their central cations [19]. It is expected that $Na_2La_2Ti_3O_{10}$ also shows pure ionic conduction. Therefore, we can give a clear discussion for the mechanism of ionic conductive behavior in the layered perovskite compounds.

In this chapter, the structure and ionic conductivity of $Na_2La_2Ti_3O_{10}$ are investigated and compared with those of niobate compounds [20] such as $NaLaNb_2O_7$ and $NaCa_2NaNb_4O_{13}$, since these two compounds in which interlayer ion environment is different from that of the Ruddlesden-Popper phase also show pure ionic conduction. On the basis of the comparison between titanate and niobate compounds, we have discussed the mechanism of ionic conductive behavior in layered perovskite compounds.

3.2 Experimental

$Na_2La_2Ti_3O_{10}$ was prepared by a solid-state reaction. The starting materials were Na_2CO_3, La_2O_3 and TiO_2. An excess amount of Na_2CO_3 (30mol%) was added to compensate for loss due to the evaporation of sodium component. The reactants were ground, pelletized and then fired in an open alumina crucible. The following three stages for the calcination were adopted in order to obtain a single phase. The mixture was fired for 12h at 550℃ in air, subsequently heated for another 6h at 1000 - 1100℃ in O_2 flow, and finally cooled slowly (<3℃ min^{-1}) to room temperature. After the reaction, the product was washed with distilled water and dried for 24h at 100℃.

Thermogravimetric analysis (TGA) and differential thermal analysis (DTA) were carried out using a Mac Science thermal analyzer system 001 at a heating rate of 5℃ min^{-1} in air. Thin specimens for electron microscopic analysis were obtained by crushing and mounting the crystal fragments on a Cu grid. Electron microscopic analysis was carried out with an ABT (Topcon) EM002B electron microscope operating at 200kV. Chemical analysis was carried out by the EDX method using an electron microscope fitted with an EDX analyzer. Powder XRD patterns were recorded on a Rigaku RAD-rA diffractometer, using Cu-K α radiation which was monochromatized by a curved crystal of graphite. The data were collected in a step-scanning mode in the 2 θ range of 5 - 100° with a step width of 0.02° and a step time of 4s. Data analysis was carried out by the Rietveld method, using the RIETAN profile refinement program [25] on an ACOS2010 computer at Niigata University. Ionic conductivity of

$Na_2La_2Ti_3O_{10}$ was measured on a pressed pellet by a complex impedance technique between 40Hz and 100kHz using a HIOKI 3520 Hi Tester in the temperature range of 300 - 800℃.

3.3 Results and Discussion

In order to obtain a monophasic $Na_2La_2Ti_3O_{10}$ compound, we first used the same method as that reported by Gondrand and Joubert [12]. However, the monophasic compound could not be obtained by their preparation conditions. The impurity phases of $La_{2/3}TiO_{3-x}$ [31] and $NaLaTiO_4$ [32] were always observed in the reaction product. After some trial and error, the preparation conditions consisting of the three steps as mentioned in the experimental section are found to be the best for the preparation of a single-phase product. In the absence of the first step, the end product is a defective perovskite, $La_{2/3}TiO_{3-x}$. The defective perovskite is considered to be more thermodynamically stable than the layered perovskite, $Na_2La_2Ti_3O_{10}$, around this temperature range. It was found that the presence of the intermediate product, $La_2O_2CO_3$, is necessary to prevent the formation of $La_{2/3}TiO_{3-x}$ in the reaction. The reaction temperature for the first step should not be permitted to exceed 600℃ because the defective perovskite is preferentially formed over this temperature. It is necessary to keep the reaction temperature for the second step within the range from 1000 to 1100℃, since the impurity phase, $NaLaTiO_4$, is produced rather than $Na_2La_2Ti_3O_{10}$ below this temperature range.

Thermogravimetric analysis indicated that $Na_2La_2Ti_3O_{10}$ does not take any hydrous form even though the compound was washed with distilled water. This result is in contrast to that of the corresponding potassium compound, $K_2La_2Ti_3O_{10}$ [13, 17], which contains 1.7 water molecules in the interlayer. Contrary to the titanate compounds, $NaLaNb_2O_7$ has 1.6 water molecules in the interlayer and $KLaNb_2O_7$ does not take any hydrous form

[19, 21]. $KLaNb_2O_7$ forms a face-centered lattice wherein potassium ions have trigonal prismatic coordination, while $NaLaNb_2O_7$ takes a body-centered lattice wherein sodium ions have almost regular tetrahedral coordinations. Therefore, the differences of the hydration behavior are due to the differences of interlayer space and not nature of interlayer cation. Since the crystal structure of $Na_2La_2Ti_3O_{10}$ and $K_2La_2Ti_3O_{10}$ are exactly the same as shown later, the hydration behavior of these compounds can be understood on the basis of the Coulomb interaction between the interlayer ions and perovskite layer. The Coulomb attractive interaction is much stronger for the sodium compound than for the of potassium compound because of the smaller ionic radius of Na^+ ions. Therefore, in the sodium compound, the energetic gains obtained by hydration of Na^+ ions do not exceed the energy required to expand the interlayer space.

Figure 3.1 shows a selected electron diffraction pattern of $Na_2La_2Ti_3O_{10}$. The indexing for each spot could be successfully accomplished in the light of analogy with the crystal structure of $Sr_4Ti_3O_{10}$ [33], one of the members of Ruddlesden-Popper phases with a tetragonal system. It was found that the incident electron beam runs along the $[\bar{1}11]$ direction and that the spots were indexed as shown in Fig. 3.1. Approximate cell parameters estimated from the diffraction pattern are a = 0.38nm and c = 2.8nm, and the reflection condition is h + k + l = 2n for (hkl) reflections. It is obvious that the doubling of the a-axis as reported by Gondrand and Joubert [12] is not observed in our result. There are two possible explanations for this disagreement. As mentioned above, the synthesis of the single-phase $Na_2La_2Ti_3O_{10}$ is achieved only under the severely controlled preparation conditions particularly in the case of heating temperatures.

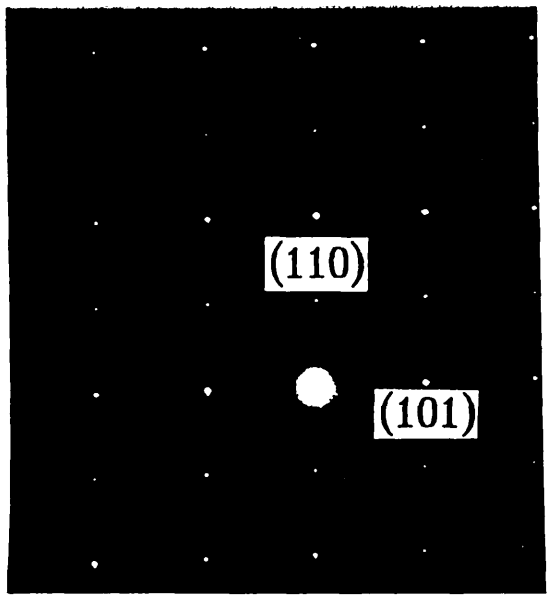

Fig. 3.1 Electron diffraction pattern of $Na_2La_2Ti_3O_{10}$.

Therefore, we suppose that some impurities may be present in their sample. In addition, the cooling rate after the high-temperature reaction may lead to some distortions of the crystal structure. Since there are no data of electron diffraction patterns and cooling rate in their paper, we do not discuss this in detail here. Figure 3.2 shows the electron micrograph of $Na_2La_2Ti_3O_{10}$ with $[\bar{1}11]$ incidence corresponding to the same zone as that of the electron diffraction pattern in Fig. 3.1. Two kinds of streaks which intersect each other with an angle nearly equal to 90° can be seen. One has a d-spacing of 0.28nm corresponding to that of the [110] direction, and the other a d-spacing of 0.38nm corresponding to that of the [101] direction. These distances coincide well with those for the edge and diagonal of a TiO_6 octahedron found in some titanates.

Indexing of the powder XRD patterns obtained was examined with the aid of the computer program CELL [24] on the basis of tetragonal symmetry. The possible space groups were chosen from the results. The reflection condition found was h + k + l = 2n for hkl reflections, which was consistent with the result for the electron diffraction. This condition led to eight possible space groups, I4, $I\bar{4}$, I4/m, I422, I4mm, $I\bar{4}m2$, $I\bar{4}2m$ and I4/mmm.

The Rietveld refinement was carried out for all of the space groups in the early refinement stages. Finally, the I4/mmm space group gives the most satisfactory fitting to the powder XRD pattern. The final reliability factors achieved were R_{wp} = 12.87%, R_p = 9.86%, R_I = 3.83%, R_F = 2.14%. The results of the pattern fitting are shown in Fig. 3.3 and the crystallographic data are listed in Table 3.1. The positional parameters and the selected

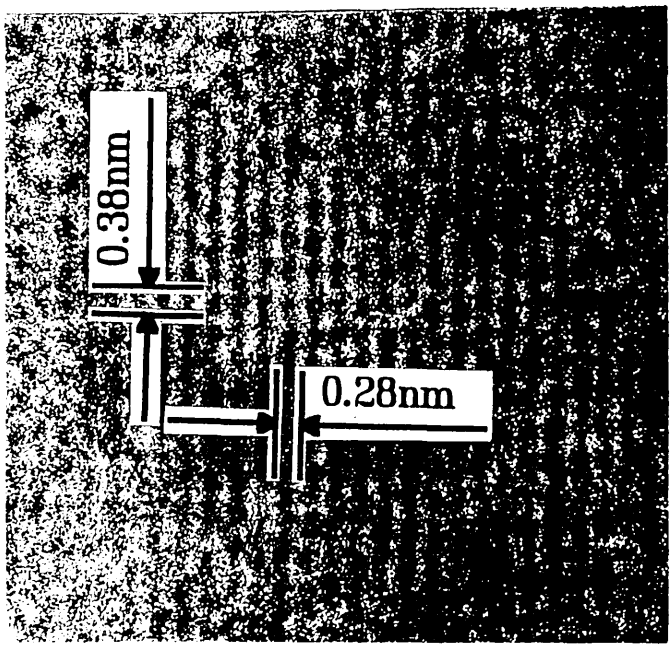

Fig. 3.2 Lattice image of [$\bar{1}$11] projection of $Na_2La_2Ti_3O_{10}$.

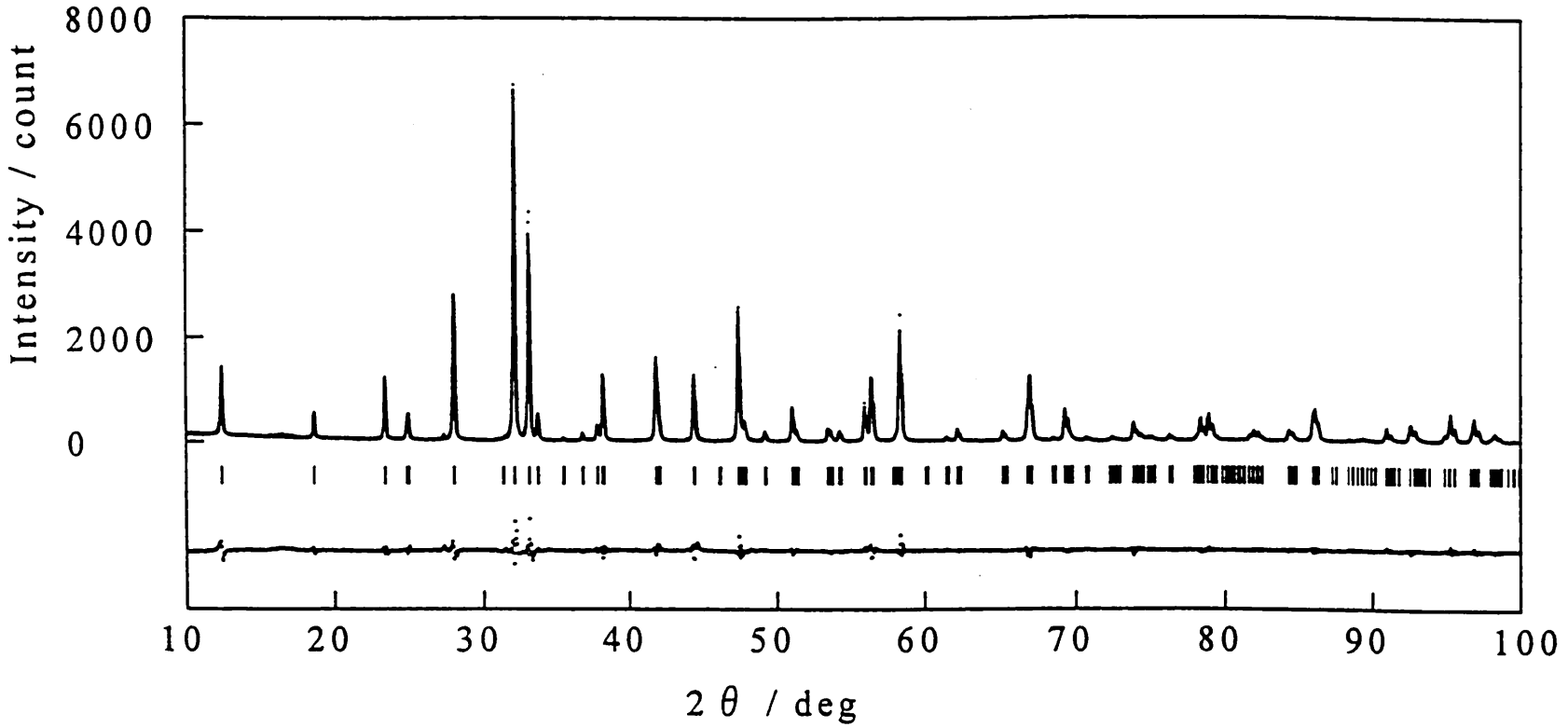

Fig. 3.3 Powder XRD pattern fitting for $Na_2La_2Ti_3O_{10}$. The calculated and observed patterns are represented by the top solid line and dots, respectively. The vertical marks in the middle show positions calculated for Bragg reflections. The trace on the bottom is a plot of the difference between calculated and observed intensities.

Table 3.1 Crystallographic data of $Na_2La_2Ti_3O_{10}$.

Radiation	CuK α
2 θ range (°)	5-100
Step scan increment (2 θ)	0.04
Count time ($s \cdot step^{-1}$)	4
Space group	I4/mmm
a (nm)	0.383528(7)
c (nm)	2.85737(7)
Volume (nm^3)	0.420301
Z	2
Calculated density ($g \cdot cm^{-3}$)	4.958
No. of reflections	195
No. of refined parameters	26
Reliable factors	$R_{wp} = 0.1287$, $R_p = 0.0986$ $R_I = 0.0383$, $R_F = 0.0214$

interatomic distances and angles are listed in Table 3.2 and Table 3.3, respectively.

The values of isotropic thermal parameters are highly scattered. In particular, the value for O(1) is considerably large, and some of values for other sites must be fixed to a positive value because of their conversion to negative values without fixing. This may be due to an insufficient correction for the preferred orientation because the prepared sample exhibits an extremely large cleavage perpendicular to the c-axis. Another origin for the scattered isotropic thermal parameters is possible, i.e., the existence of intergrowth. There have been many studies on the intergrowth of titanate compounds [3, 34, 35]. However, this phenomenon is very troublesome and has not yet been clarified theoretically. The information of short-range disorder of the crystal structure cannot be obtained by powder XRD pattern analysis. Another approach, for example, high-resolution electron microscopic study, is necessary to determine intergrowth occurs in this material.

The crystal structure of $Na_2La_2Ti_3O_{10}$ is illustrated in Fig. 3.4. The structure is composed of a perovskite unit with three layers and a rock-salt-type unit (NaO) stacked alternately along the c-axis. The adjacent triple perovskite sheets, $La_2Ti_3O_{10}$, are stacked with a displacement by 1/2 along the (110) direction. A sodium ion in this compound occupies the nine-fold sites between the two perovskite layers. A lanthanum ion occupies the twelve fold sites in the center of the perovskite lattice. The feature of the crystal structure in this compound is the same as those of proton, potassium and silver compounds [13, 17]. The relative arrangement of the adjacent perovskite sheets is independent of its ionic size while existing in the

Table 3.2 Positional parameters of $Na_2La_2Ti_3O_{10}$.

Atom	Site[a)]	g[b)]	x	y	z	B / nm^2
Na	4e	1.0	0.0	0.0	0.2895(9)	0.005
La	4e	1.0	0.0	0.0	0.4246(1)	0.0006(11)
Ti(1)	2a	1.0	0.0	0.0	0.0	0.001
Ti(2)	4e	1.0	0.0	0.0	0.1491(4)	0.001
O(1)	4c	1.0	0.0	0.5	0.0	0.080(20)
O(2)	4e	1.0	0.0	0.0	0.065(1)	0.005
O(3)	8g	1.0	0.0	0.5	0.137(1)	0.004(6)
O(4)	4e	1.0	0.0	0.0	0.210(1)	0.008(8)

a) Multiplicity and Wyckoff notation.
b) Occupancy.

Table 3.3 Bond distances (nm) and angles (°) of $Na_2La_2Ti_3O_{10}$.

Distance		Angle	
Na - O(4)	0.2278(43)	O(2) - Ti(2) - O(3)	79.4(8)x4
Na - O(4)[i)]	0.27120(4)x4	O(4) - Na - O(4)	90.2(5)x4
Na - O(3)[i)]	0.2854(28)x4		
La - O(1)[i)]	0.2884(3)x4		
La - O(2)[i)]	0.2729(4)		
La - O(3)[i)]	0.2594(19)		
Ti(1) - O(1)	0.1918(0)x4		
Ti(1) - O(2)	0.1848(35)x2		
Ti(2) - O(2)	0.2412(37)		
Ti(2) - O(3)	0.1951(5)x4		
Ti(2) - O(4)	0.1734(38)	Symmetry code	
O(1) - O(1)[ii)]	0.2712(0)x4		
O(1) - O(2)	0.2663(24)x4	None	x, y, z
O(2) - O(3)	0.2809(32)x4	i)	1/2-x, 1/2-y, 1/2-z
O(3) - O(3)[ii)]	0.2712(0)x4	ii)	-y, x, z
O(3) - O(4)	0.2839(36)x4		

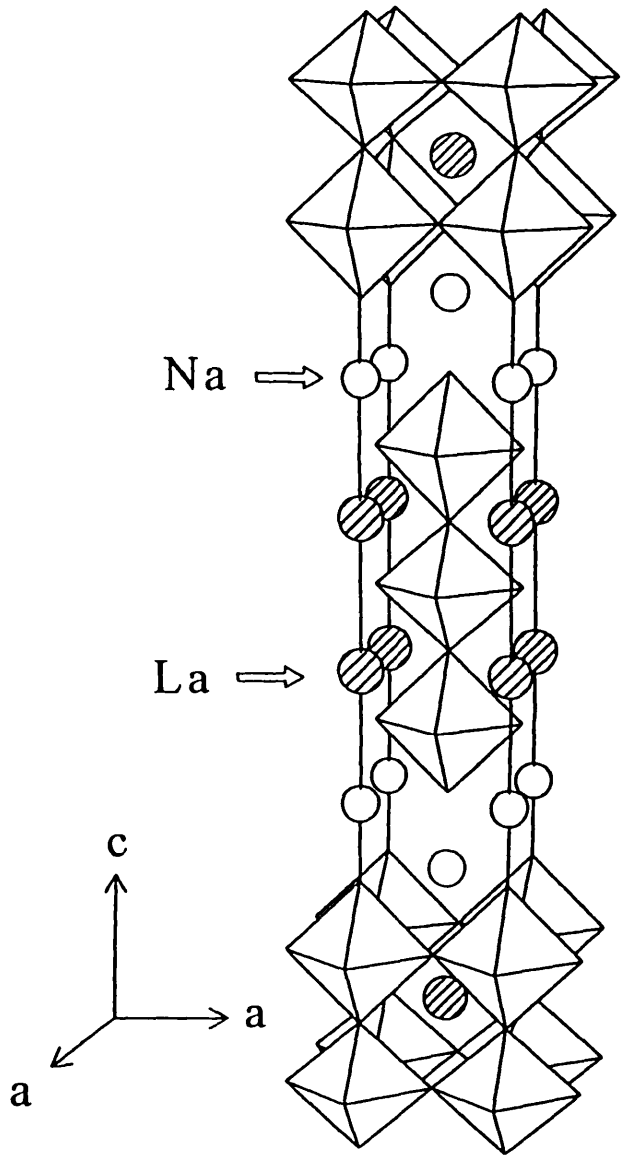

Fig. 3.4 Crystal structure of $Na_2La_2Ti_3O_{10}$. The octahedra are TiO_6 units.

interlayer. This stacking feature is in contrast to that of niobate compounds [21]. In niobate oxides with a layered perovskite structure, only one sodium ion can be accommodated in the interlayer space per NbO_6 octahedron located toward the space. No matter how many perovskite layers are constructed, such $NaLaNb_2O_7$, $NaCa_2Nb_3O_{10}$, and $NaCa_2NaNb_4O_{13}$, this is always true due to the high positive charge of the central ion of the NbO_6 octahedron. This situation can lead to a lower charge density state for the interlayer space. As the result, the Coulomb interaction between the perovskite layer and the interlayer ion is relatively weak, reflecting a variety of stacking features of the adjacent perovskite layer blocks owing to the ionic size of the interlayer ions. On the other hand, in titanate oxides, the lower charge of the central ion of the TiO_6 octahedron is compensated by two interlayer monovalent ions per TiO_6 octahedron located toward the interlayer, i.e., a high positive charge density state is realized in the interlayer space. This is consistent with the fact that $Na_2La_2Ti_3O_{10}$ crystal is stable upon the irradiation of a high-energy electron beam in the electron microscopy studies.

Figure 3.5 shows the environment of titanium atoms in $Na_2La_2Ti_3O_{10}$. A large distortion of the TiO_6 octahedra exists in the structure. The TiO_6 octahedron located inside of the perovskite layers is close to an ideal octahedron, while those located outside of the layer are fairly distorted. The oxygen with a fairly shortened distance of Ti-O is located toward sodium ions between the triple perovskite layers. These bond characters are similar to those of $NaLaNb_2O_7$ [19]. The distortion of metal-oxygen octahedra in the perovskite layer is a quite common feature observed in layered perovskites which exhibit an ion-exchange property [17, 19]. Such shortness of the

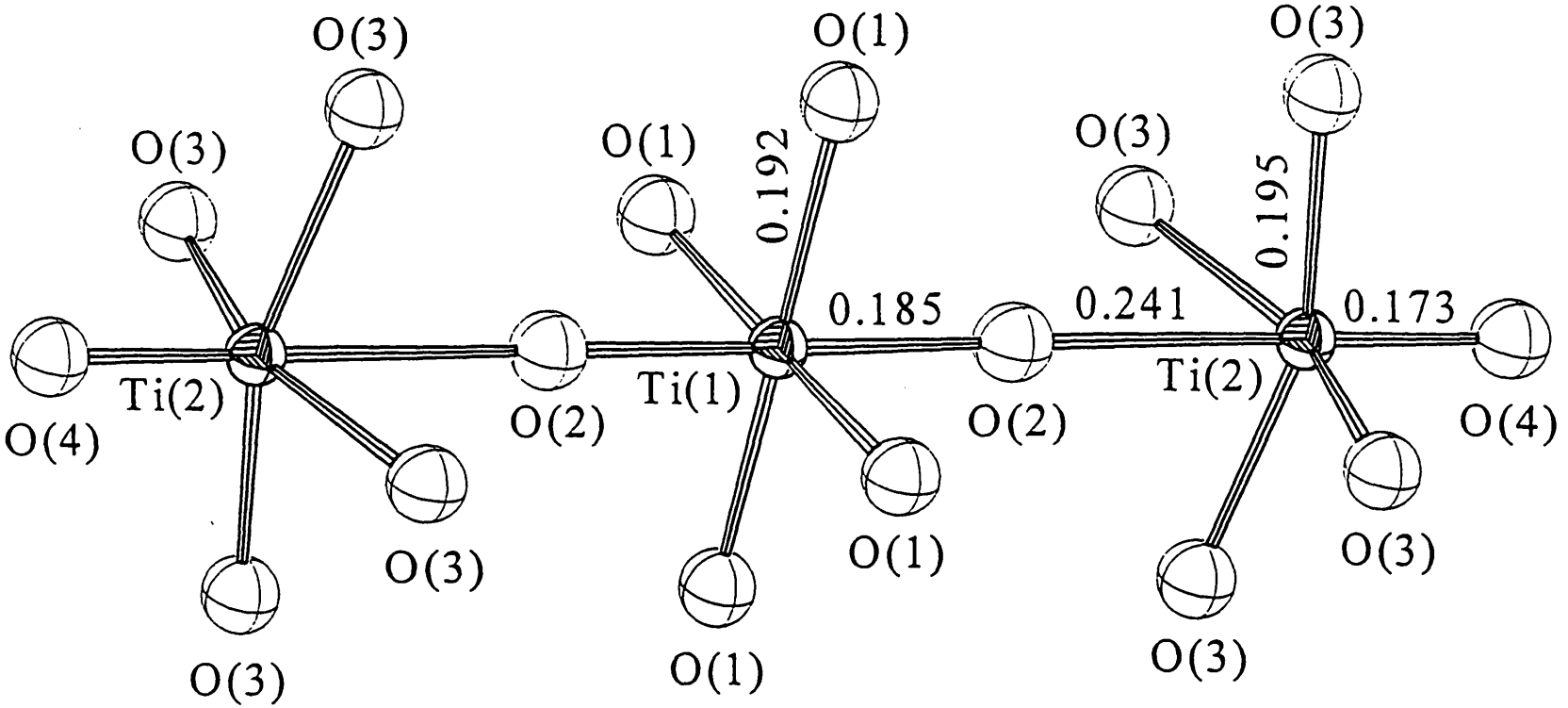

Fig. 3.5 Environment around titanium atoms in the perovskite layer of $Na_2La_2Ti_3O_{10}$.

Ti-O distance seems to cause less interaction between the sodium and the crystal lattice of the sheets. Therefore, it is possible in this situation to exchange the ions in the interlayer with other alkali ions and protons as reported previously [12, 13, 17].

Figure 3.6 shows the ionic conductivity of $Na_2La_2Ti_3O_{10}$ as a function of temperature. A sharp drop of ionic conductivity was observed at around 575℃. Since the X-ray powder pattern above this temperature showed the formation of the defective perovskite, $La_{2/3}TiO_{3-x}$, in this sample, this change is due to the decomposition of $Na_2La_2Ti_3O_{10}$. It is interesting to compare the ionic conductivity of $Na_2La_2Ti_3O_{10}$ with those of niobate compounds. The value of ionic conductivity of $Na_2La_2Ti_3O_{10}$ is approximately 10 times less than those of niobate compounds, $NaLaNb_2O_7$ and $NaCa_2NaNb_4O_{13}$ [20]. These results are analogous to those obtained using the silver-exchange compounds [17]. Such difference in the ionic conductivity between the titanate and the niobate compounds is due to the difference in the charge density of the interlayer contributed by the central ions (Ti^{4+} and Nb^{5+}) of the TiO_6 and NbO_6 octahedra. The common features among sodium and silver compounds are due to the similarity of their crystal structure. The high charge density in the interlayer of titanate compounds leads to strong electrostatic interaction between the perovskite layer. The environment of the sodium atoms in $Na_2La_2Ti_3O_{10}$ is illustrated in Fig. 3.7. Here, sodium ions are situated in a rigid rock-salt-type coordination with 100% occupancy. On the other hand, sodium ions in $NaLaNb_2O_7$ and $NaCa_2NaNb_4O_{13}$ are located in a tetrahedral coordination with 50% occupancy. Therefore, the ionic motion in $Na_2La_2Ti_3O_{10}$ is more tightly restricted than those of $NaLaNb_2O_7$ and $NaCa_2NaNb_4O_{13}$. The

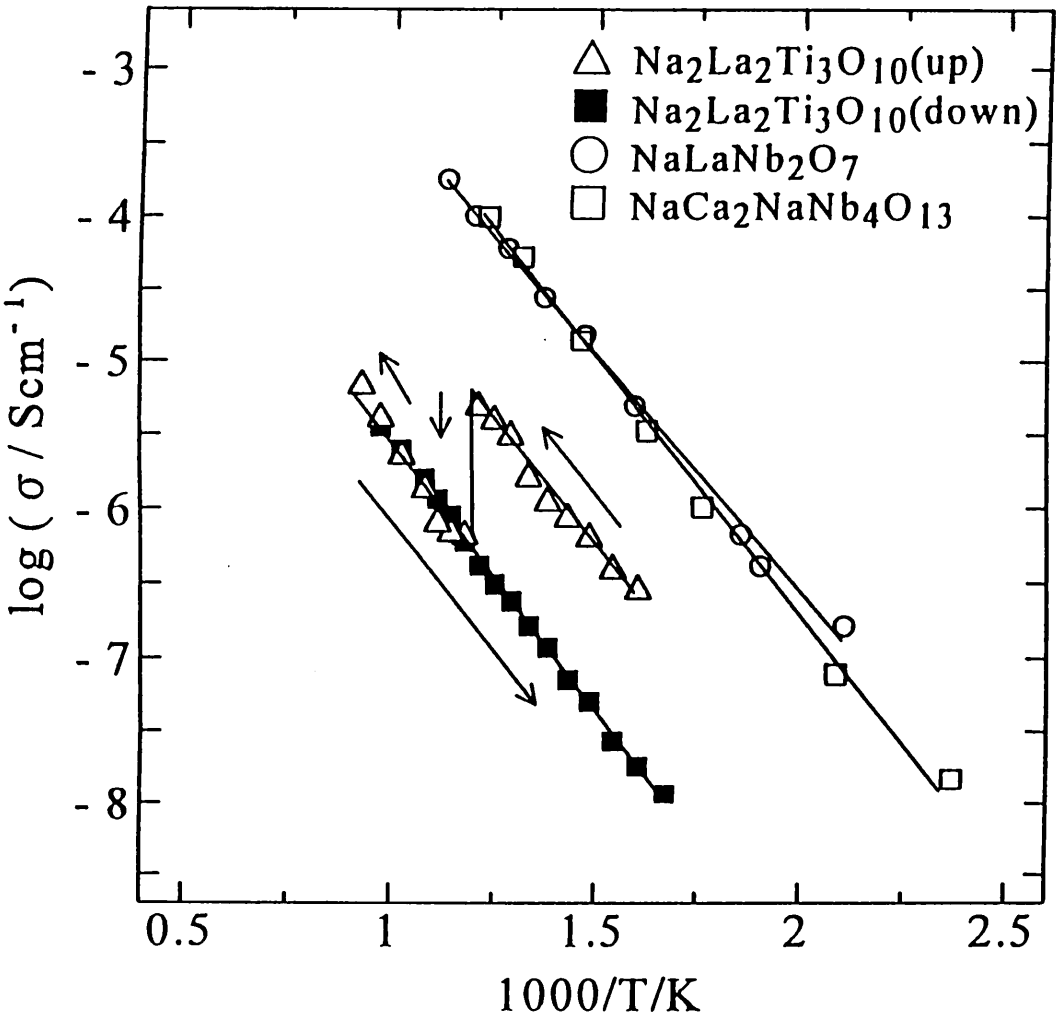

Fig. 3.6 Temperature dependence of ionic conductivity of $Na_2La_2Ti_3O_{10}$, $NaLaNb_2O_7$ and $NaCa_2NaNb_4O_{13}$. (▲) represents data for temperature increasing direction and (●) for temperature decreasing direction.

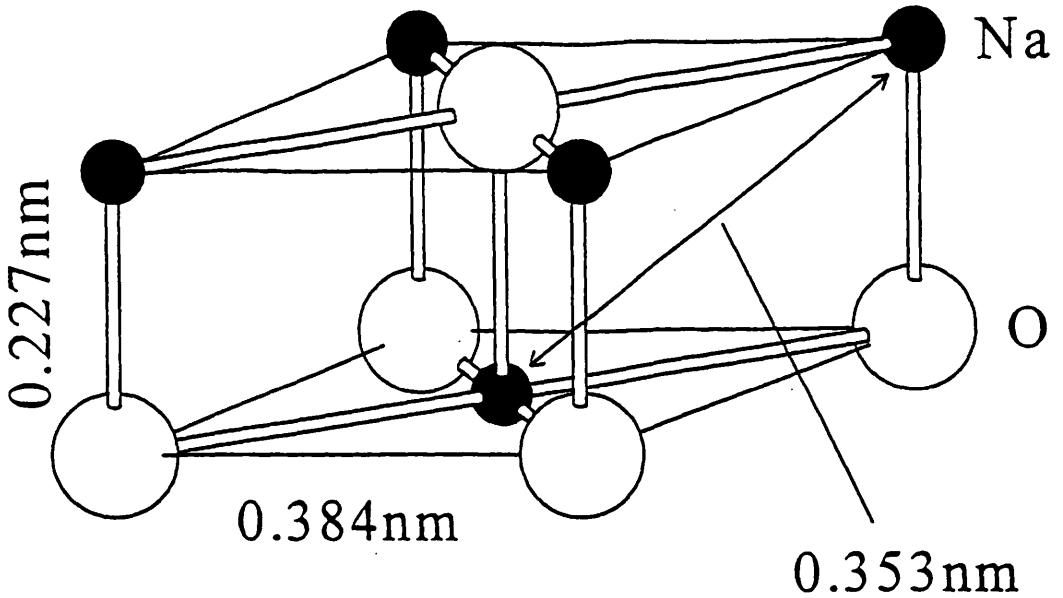

Fig. 3.7 Environment around sodium atoms in $Na_2La_2Ti_3O_{10}$.

differences of coordination around sodium ion reflect the differences of ionic conductivity between the titanate and niobate compounds. These results indicate that the ion conducting behavior in the layered perovskite compounds is mainly dependent upon the environment around the conductive ions in the interlayer [20].

3.4 Summary

An ion-exchangeable layered perovskite compound, $Na_2La_2Ti_3O_{10}$, was directly synthesized by a solid-state reaction. The crystal structure of $Na_2La_2Ti_3O_{10}$ was determined by electron diffraction analysis and Rietveld analysis for the powder XRD pattern. The unit cell is tetragonal with a = 0.383528(7)nm, c = 2.85737(7)nm and Z = 2 with the space group I4/mmm (No. 139). The structure of this compound is analogous to that of the Ruddlesden-Popper phases. The ionic conductivity of $Na_2La_2Ti_3O_{10}$ was not very high compared with those of niobate compounds, $NaLaNb_2O_7$ and $NaCa_2NaNb_4O_{13}$. Such a low ionic conductivity is due to the rigid rock-salt-type coordination around sodium ions located at the interlayer.

Chapter 4

Crystal Structure Determination of Layered Perovskites Compounds, $NaLnTiO_4$ (Ln = La, Eu, Gd, Y, and Lu)

4.1 Introduction

The layered perovskite compounds, $NaLnTiO_4$ (Ln = lanthanide), was first prepared by Blasse [32]. Its X-ray powder diffraction pattern was successfully indexed as a tetragonal unit cell. It has been estimated on the basis of indexing of XRD pattern that the interlayer cations in $NaLnTiO_4$ are ordered between the two available interlayer sites. However, there has been no direct evidence that such ordering really exist.

In this chapter, we present the synthetic conditions required for the formation of $NaLnTiO_4$ and discuss the proposed structure of these compounds including an analysis of the relative sizes of the rare earth ions and the alkali metal cations required for the stabilization of the structure. This compound is of interest because it is the only $AA'BO_4$ compound that contains ordering A-site cations.

4.2 Experimental

$NaLnTiO_4$ was prepared by conventional solid-state reaction. The starting materials were mixture of Na_2CO_3, Ln_2O_3, TiO_2 powder. An excess amount of Na_2CO_3 (30mol%) was added to compensate for the loss due to the evaporation of sodium component. Sodium carbonate can also be acted as oxidizing flux [36]. The reactants were ground, pelletized and then fired in an open alumina crucible. The mixture was fired at 900-1000℃ for Ln = La - Gd and at 1050℃ for Ln = Y and Lu in air. The samples were heated for 30 min at above temperatures.

Powder XRD patterns were recorded on a Rigaku RAD-rA diffractometer, using Cu-K_α radiation which was monochromatized by a curved crystal of graphite. The data were collected by a step-scanning mode in the 2θ range of 5 - 100° with a step width 0.02° and a step time 4s. Indexing of the powder XRD patterns obtained was examined with the aid of the computer program CELL [24]. Structural refinements were performed with a Rietveld program RIETAN [25] on an ACOS2010 computer at Niigata University.

4.3 Results and Discussion

The preparation of $NaLnTiO_4$ has been described previously by Blasse [32] and Linares and Blanchard [37]. First the $NaLnTiO_4$ was prepared by the method similar to synthetic conditions of them. The resulting products were not single-phase but a mixture of $NaLnTiO_4$ and $Na_2Ln_2Ti_3O_{10}$. The synthetic conditions of $NaLnTiO_4$ were investigated in detail to obtain single phase materials. In the search for appropriate synthetic conditions, we found that $Na_2Ln_2Ti_3O_{10}$ is preferentially formed in high reaction temperatures. To prepare single phase $NaLnTiO_4$, the reaction conditions had to be modified slightly. A low reaction temperature was necessary to obtain the single-phase. The reaction temperatures was decreased to 900 - 1000℃ for Ln = La - Gd and 1050℃ for Ln = Y. It is necessary to keep the reaction temperature within the range from 900 to 1000℃ for Ln = La - Gd and 1050℃ for Ln = Y, since the intermediate compound is remained below this temperature range. The diffraction pattern of the intermediate compound can be indexed using an orthorhombic cell with lattice parameters related to those of a pseudo-cubic perovskite by $2^{1/2}a_p \times 2^{1/2}a_p \times 2a_p$, where a_p is the lattice parameter of the pseudocubic structure. The thermal stability of the intermediate compound is very sensitive to the size of rare earth ions. The decomposition temperature of intermediate compound increase with the replacement of a larger rare earth with a smaller one. For example, the intermediate compounds of Ln = Eu were decomposed by heating at about 850℃, whereas those of Ln = Y were decomposed at about 1050℃. Therefore, the single phase compound of Ln = Lu could not be obtained by the above preparation conditions because of the

high decomposition temperature of the intermediate compound. An extended heat treatment at a low reaction temperature (e.g. 900℃) was unfavorable. The product showed an asymmetric broadening toward the lower side diffraction angle of the XRD pattern. It seems that the broadening is caused by a structural disorder of interlayer cations. As mentioned above, the single-phase sample of $NaLnTiO_4$ was obtained for the quite limited preparation conditions.

In the earlier study [37], the space group of $NaLnTiO_4$ (Ln = rare earths) was reported to be P4mm with a tetragonal symmetry, although the refinement of the crystal structure was unsuccessful. Linares and Blanchard [38] pointed out that the symmetry of the rare earth site in the $NaLnTiO_4$ (except for Ln = La) is lower than C_{4v} because the number of lines observed in the emission spectra of $NaLnTiO_4$:Eu is much more than those expected usually from the symmetry C_{4v}. Therefore, we reexamined the indexing of the XRD patterns of $NaLnTiO_4$ by means of the CELL program. For Ln = La, the XRD pattern exhibits the simple diffraction pattern without superlattice reflection. The pattern of $NaLaTiO_4$ indicates that hk0 reflections with h + k = 2n + 1 are systematically absent. All the peaks in the XRD pattern of $NaLaTiO_4$ can be indexed by a tetragonal cell with P4/nmm space group. On the other hand, the XRD patterns for Ln = Eu - Lu are readily distinguishable from the tetragonal phase. The XRD patterns showed weak extra reflections which could not be explained in accordance to the tetragonal cell with P4mm or P4/nmm space group. These results clearly indicate that $NaLnTiO_4$ (Ln = Eu - Lu) have a lower symmetry than tetragonal one. The reflection conditions found are k = 2n for 0kl and 0k0 reflections and l = 2n for h0l and 00l reflections on the basis of an

orthorhombic symmetry. These conditions lead to Pbcm and $Pbc2_1$ space groups. In this study, we adopted Pbcm space group with higher symmetry than $Pbc2_1$, because some of the standard deviations for structural parameters became fairly large (sometimes the order of about 10^{-2}) in the case of $Pbc2_1$ space group for the Rietveld refinement. This space group explains the weak reflections in the XRD patterns. As an example, the results of the pattern fitting for $NaLaTiO_4$ and $NaEuTiO_4$ are shown in Figs. 4.1 and 4.2. The structural models for $NaLaTiO_4$ and $NaEuTiO_4$ are illustrated in Fig. 4.3 and 4.4. The crystallographic data finally obtained from the Rietveld refinement are listed in Tables 4.1. The atomic coordinates are very precise, but the atomic temperature factors B are less so. We note that the Bragg peaks with strong l character were fit relatively poorly compared with other peaks. Such discrepancies could result from the occurrence of some stacking faults and a structural disorder in this layered structure due to a long periodicity of the stacking direction of perovskite slab.

It is interesting to examine the variation of the lattice parameters and c/a ratios in $NaLnTiO_4$ type compounds with the size of the rare earth ion. The c/a ratio is a useful parameter in determining the structure type of K_2NiF_4 phase. The variations of lattice parameter c and c/a ratio are illustrated in Fig. 4.5. The variation of lattice parameter a with the size of the rare earth ions is smaller than that of c/a ratio. Substitution of La^{3+} by the smaller rare earth ions leads to a decrease in lattice parameter c and c/a ratio. If the BO_6 octahedra were regular and all the A-O distances were identical in the A_2BO_4 compound, the theoretical value of c/a ratio is 3.41. In general, c/a ratio of K_2NiF_4-type compound is usually found to be $3.30 \pm$

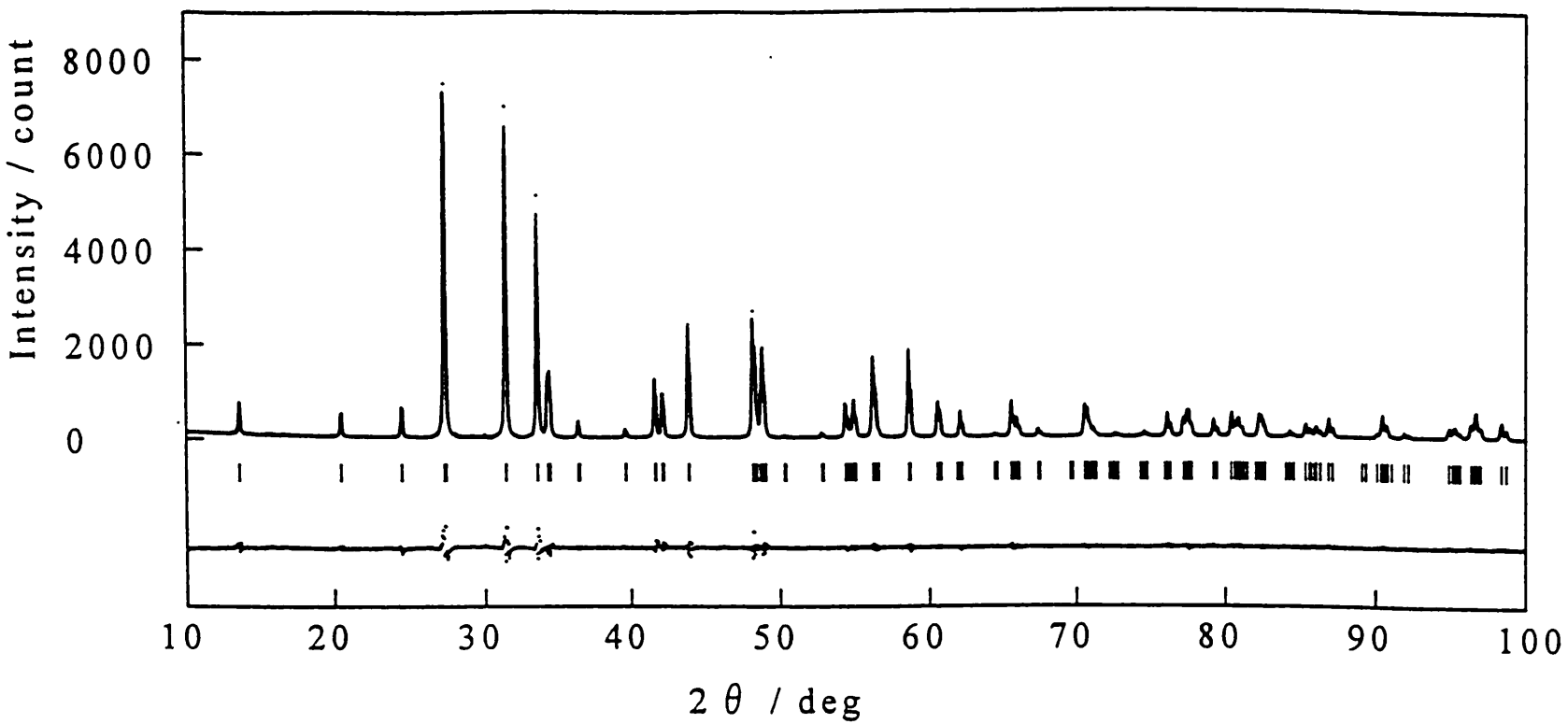

Fig. 4.1 X-ray powder pattern fitting for $NaLaTiO_4$. The calculated and observed patterns are shown on the top solid line and the dots, respectively. The vertical marks in the middle show positions calculated for Bragg reflections. The trace on the bottom is a plot of the difference between calculated and observed intensities.

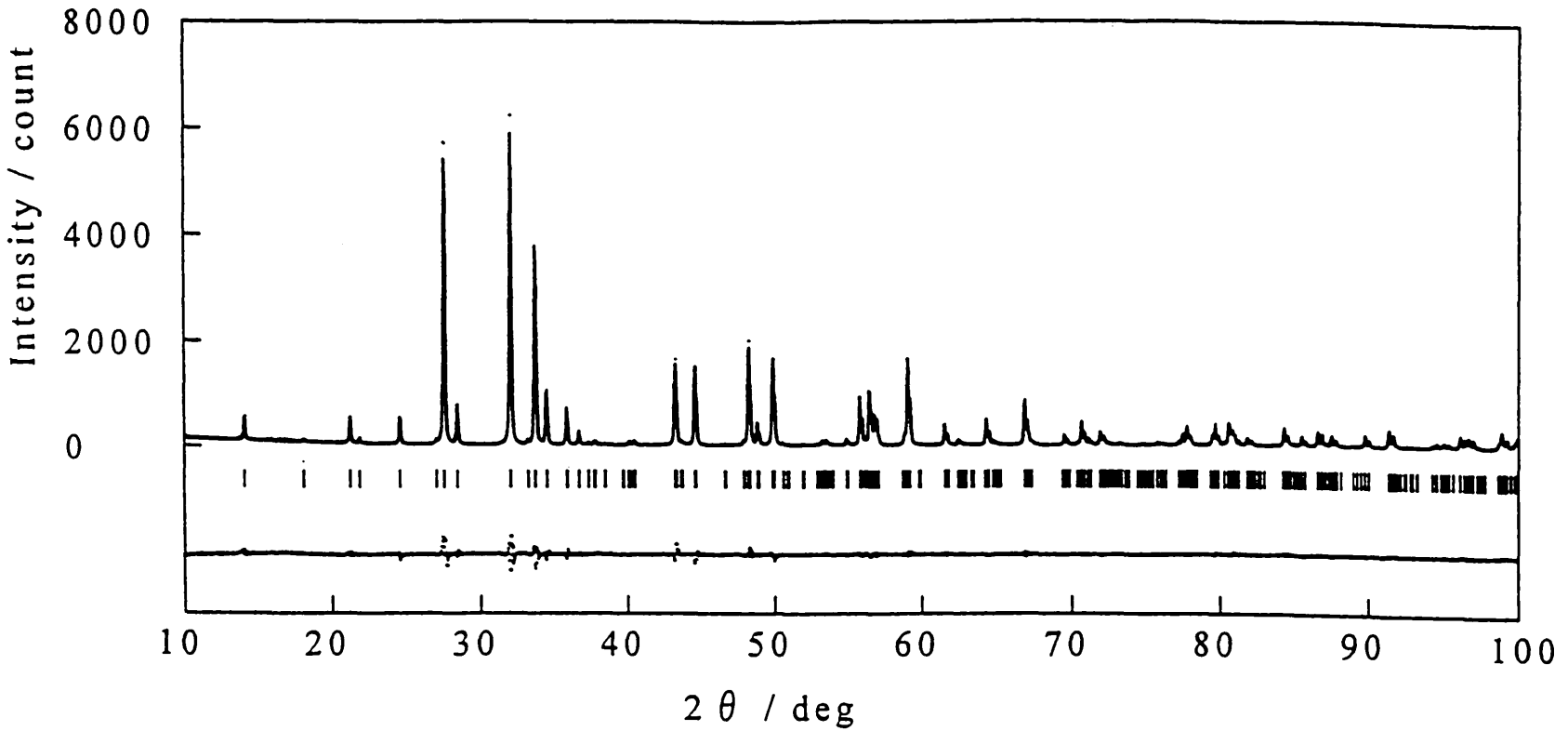

Fig. 4.2 X-ray powder pattern fitting for $NaEuTiO_4$.

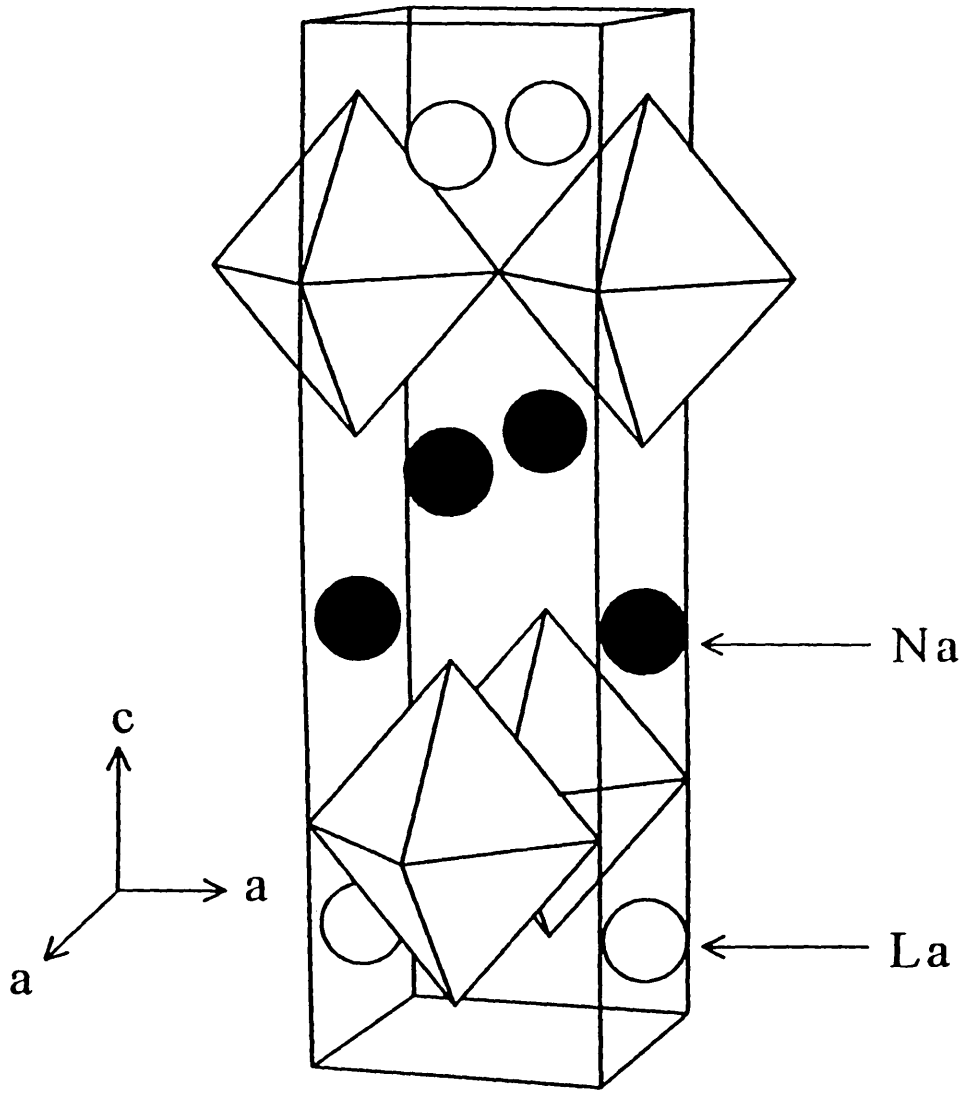

Fig. 4.3 Structural model of $NaLaTiO_4$.

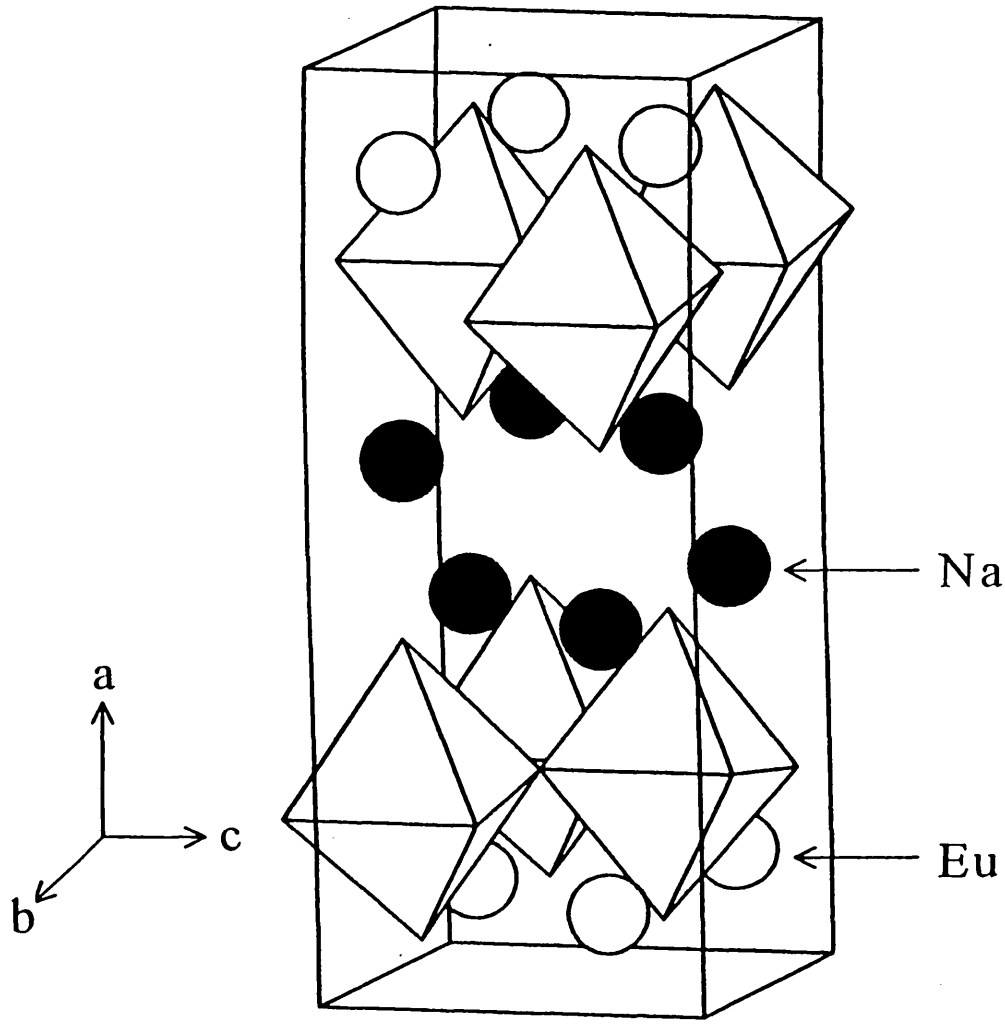

Fig. 4.4 Structural model of $NaEuTiO_4$.

Table 4.1 Crystallographic data for $NaLnTiO_4$ (Ln = La, Eu, Gd, and Y).

Sample	Atom	Site[a)]	x	y	z	B / nm²
$NaLaTiO_4$	Na	2c	0.0	0.5	0.585(1)	0.015(4)
P4/nmm (No. 129)	La	2c	0.0	0.5	0.8890(2)	0.001
a = 0.377404(5)nm	Ti(1)	2c	0.0	0.5	0.2755(6)	0.001
c = 1.30146(3)nm	O(1)	2c	0.0	0.0	0.243(1)	0.003(4)
R_{wp} = 11.01%	O(2)	2c	0.0	0.5	0.072(2)	0.002(6)
R_F = 2.58%	O(3)	4d	0.0	0.5	0.406(2)	0.006(6)
$NaEuTiO_4$	Na	4d	0.5876(9)	0.0118(35)	0.25	0.010(3)
Pbcm (No. 57)	Eu	4d	0.8925(2)	0.0185(5)	0.25	0.002(1)
a = 1.25436(2)nm	Ti(1)	4d	0.2664(4)	0.0069(18)	0.25	0.005
b = 0.53285(4)nm	O(1)	4c	0.2190(19)	0.25	0.0	0.015(8)
c = 0.53281(4)nm	O(2)	4c	0.7547(18)	0.25	0.0	0.003(6)
R_{wp} = 10.80%	O(3)	4d	0.0711(16)	-0.0536(45)	0.25	0.005
R_F = 2.09%	O(4)	4d	0.3996(15)	0.0386(44)	0.25	0.005
$NaGdTiO_4$	Na	4d	0.5896(11)	0.0157(41)	0.25	0.008(3)
Pbcm (No. 57)	Gd	4d	0.8925(2)	0.0217(6)	0.25	0.001(1)
a = 1.24727(4)nm	Ti(1)	4d	0.2652(5)	0.0075(21)	0.25	0.005
b = 0.53349(6)nm	O(1)	4c	0.2130(20)	0.25	0.0	0.015(8)
c = 0.53361(5)nm	O(2)	4c	0.7570(21)	0.25	0.0	0.005
R_{wp} = 10.40%	O(3)	4d	0.0716(18)	-0.0729(63)	0.25	0.007(8)
R_F = 1.73%	O(4)	4d	0.3970(16)	0.0368(53)	0.25	0.005
$NaYTiO_4$	Na	4d	0.5905(9)	0.0154(36)	0.25	0.023(3)
Pbcm (No. 57)	Y	4d	0.8931(2)	0.0298(8)	0.25	0.004(1)
a = 1.22134(3)nm	Ti(1)	4d	0.2610(5)	0.0111(17)	0.25	0.005(1)
b = 0.53517(3)nm	O(1)	4c	0.2062(16)	0.25	0.0	0.010(6)
c = 0.53509(3)nm	O(2)	4c	0.7571(17)	0.25	0.0	0.010(6)
R_{wp} = 9.75%	O(3)	4d	0.0703(15)	-0.0809(50)	0.25	0.012(7)
R_F = 2.25%	O(4)	4d	0.3980(14)	0.0568(49)	0.25	0.011(5)

a) Multiplicity and Wyckoff notation.

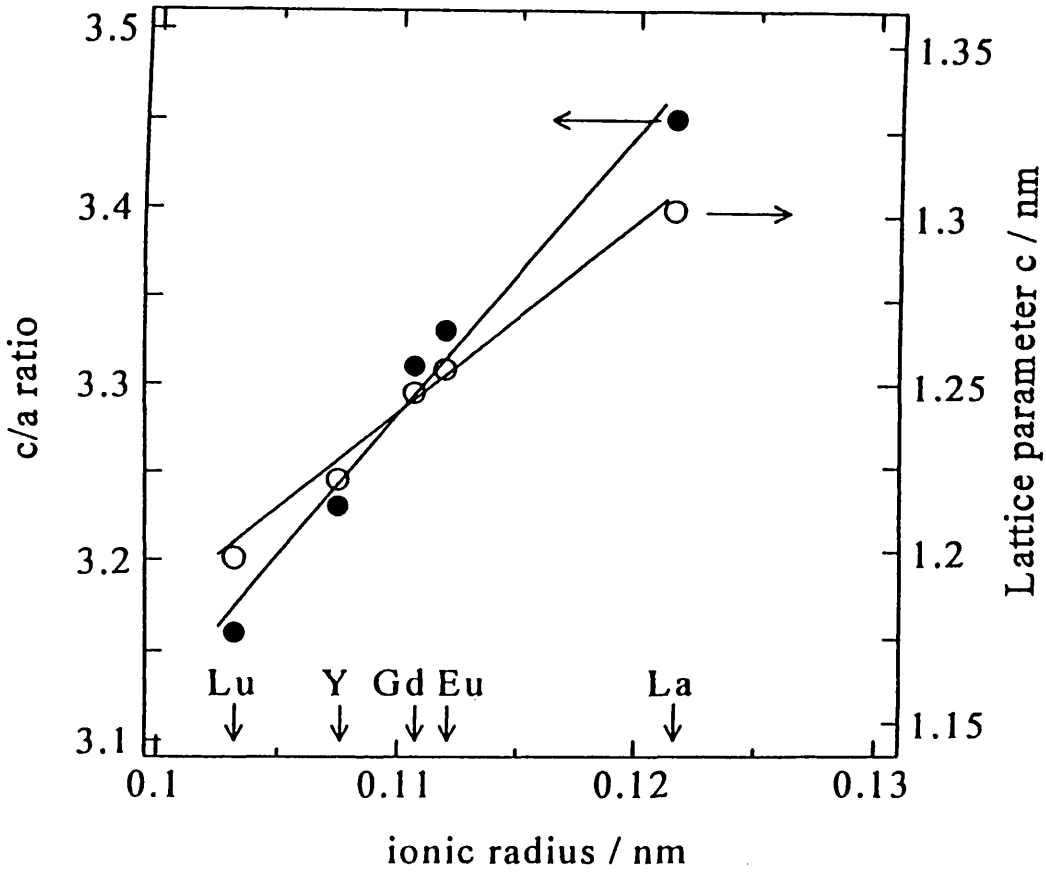

Fig. 4.5 Variation of lattice parameter c and c/a ratio in $NaLnTiO_4$ (Ln = La, Eu, Gd, Y, and Lu) as a function of ionic radius of rare earth ion. The value of c/a ratio for the orthorhombic samples were calculated using the value of primitive cell.

0.1 [9]. $NaLaTiO_4$ and $NaLuTiO_4$ have unusually high (3.45) and low (3.16) c/a ratio, respectively. If the octahedra in tetragonal $NaLaTiO_4$ are regular, the cell parameter a would be in the range 0.390 - 0.396nm. The observed value (0.377nm) is much smaller. Ganguly and Rao presumed from data of the lattice parameters of $NaLaTiO_4$ that there is a considerable pressure on the Ti-O equatorial distances of the TiO_6 octahedra in $NaLaTiO_4$ [9]. As shown in the refinement results of the crystal structure for $NaLaTiO_4$, this apparent compressed bond is due to the deviation of titanium ion from the octahedral center. The Ti-O equatorial distance (0.1935(4)nm) is similar to that observed for Sr_2TiO_4, in contrast to the Ti-O apical distances with abnormally short (0.170(2)nm) and long bond (0.265(2)nm). In $NaLnTiO_4$, the charge imbalance between Na^+ and Ln^{3+} ions both located in the interlayer is compensated by a displacement of the Ti^{4+} ions from the position of the regular octahedral center toward the Na^+ ions. Such a distortion of TiO_6 octahedra in their compounds is contrasted to that of Ruddlesden-Popper phase, $Sr_3Ti_2O_7$, which has an almost regular TiO_6 octahedral structure [39]. Blasse and Van Den Heuvel suggested from the infrared and Raman spectra of $NaLnTiO_4$ (Ln = La, Gd and Y) that the position of Ti atom in the TiO_6 octahedra is shifted from a regular central position [37]. Our structure refinement results obtained here strongly supports their prediction. The stability of A_2BO_4 structure is often describe in terms of a tolerance factor defined as [7]

$$t = (r_A + r_O) / \sqrt{2}\,(r_B + r_O) \qquad (4 - 1)$$

where $r_A + r_O$ and $r_B + r_O$ refer to the sum of the ionic radii of A-O and B-O bonds. Based on Shannon's ionic radii, the calculated tolerance factors of $NaLaTiO_4$ are 0.94 and 0.93. Since the Ti-O-Ti bond is bent considerably from the ideal bond angle of 180°, the effective Ti-O bond distance is reduced. Therefore, the tolerance factors of $NaLaTiO_4$ are close to unity required from the ideal tetragonal geometry. This result is consistent with the fact that the space group of $NaLaTiO_4$ was P4/nmm with a tetragonal symmetry. The tolerance factor also explains the change of the symmetry from tetragonal to orthorhombic for $NaLnTiO_4$ (Ln = Eu - Lu). The occurrence of the orthorhombic symmetry is ascribable to the tilting of TiO_6 octahedra. The decrease in tolerance factor with a decrease of the ionic radius of rare earth ions causes the mismatch between TiO_2 and LnO_2 layers. Considerable energy to stretch the Ln-O bond in a bilayer of LnO would be required because of the high charge of the Ln^{3+} ions. On the other hand, the Na-O interaction is weaker than the Ln-O interaction. As a result, the mismatch between TiO_2 and LnO_2 layers is compensated by the tilting of TiO_6 octahedra.

4.4 Summary

The layered perovskite compounds, $NaLnTiO_4$ (Ln = La, Eu, Gd, Y, and Lu), were synthesizes by a solid state reaction. The crystal structure of these compounds were determined by Rietveld analysis for the XRD pattern. For Ln = La - Y, it can be synthesized only under very narrowly defined conditions. The composition of $NaLuTiO_4$ was not single phase under the conditions used in this study. The stabilization of the $NaLnTiO_4$ structure were discussed on the basis of an analysis of the relative sizes of the rare earth ions and the alkali metal cations. By using two parameters, i.e., c/a ratio and tolerance factor t, the change of the crystal symmetry can be explained. The lowering of the symmetry are considered to be introduced by the mismatch between TiO_2 and LnO_2 layers.

Chapter 5

Synthesis of Novel Intercalation Compounds, $AgLnTiO_4$ and $LiLnTiO_4$ (Ln = La and Eu)

5.1 Introduction

Ion-exchange reactions in inorganic solids can be used to provide metastable phases. An example is the synthesis of novel solid Brönsted acids, $H_2Ln_2Ti_3O_{10}$ (Ln = rare earth), from $A_2Ln_2Ti_3O_{10}$ (A = K, Rb, Cs) by ion-exchange reaction [13]. In chapter 4, the crystal structure of layered perovskite compound, $NaLnTiO_4$, were determined [40]. These compounds show a sequential ordering of the cations in such a way as [-Ln-Ln-Na-Na-]. Although the characteristics of the crystal structure in these compounds are similar to the ion-exchangeable triple layered perovskite compounds [21, 41], the ion-exchange reaction of the layered perovskites, $NaLnTiO_4$, has not been reported. If the ion-exchange reaction is taken place in these layered perovskite compounds, their physical properties could be controlled by the exchanged ions.

In this chapter, we report the synthesis of novel compounds, $AgLnTiO_4$ and $LiLnTiO_4$ (Ln = La and Eu), by ion-exchange reaction from parent sodium compounds.

5.2 Experimental

The parent compounds, $NaLaTiO_4$ and $NaEuTiO_4$, were prepared as described in chapter 4. $AgLnTiO_4$ and $LiLnTiO_4$ have been prepared by the ion-exchange reaction from parent compounds, $NaLnTiO_4$ (Ln = La and Eu). Silver and lithium exchange of interlayer sodium ions in sodium compounds were carried out in molten $AgNO_3$ at 250℃ for 12h and $LiNO_3$ at 310℃ for 12h, respectively. After the reaction, the precipitate of silver compound was collected, washed with distilled water and then with ammonia solution in order to eliminate silver oxide, Ag_2O. The product was washed with distilled water again and air-dried at room temperature. The completion of the ion-exchange reaction was confirmed by XRD and X-ray fluorescence analyses.

Powder XRD patterns were recorded on a Rigaku RAD-rA diffractometer, using Cu-K_α radiation which was monochromatized by a curved crystal of graphite. The data were collected by a step-scanning mode in the 2θ range of 5 - 100° with a step width 0.02° and a step time 4s. Indexing of the powder XRD patterns obtained was examined with the aid of the computer program CELL [24]. Data analysis was carried out by the Rietveld method, using the RIETAN profile refinement program [25] on an ACOS2010 computer at Niigata University.

5.3 Results and Discussion

As shown refinement of crystal structure in chapter 4, the charge imbalance between sodium and lanthanide ions in $NaLnTiO_4$ is compensated by a displacement of the titanium ions from the position of a regular octahedral center toward the sodium ions. The oxygen with a fairly shortened distance of Ti-O is located toward sodium ions between the perovskite layers. These bond characters are similar to those of $Na_2La_2Ti_3O_{10}$. An important common structural feature of all the series of ion-exchangeable layered perovskite compounds is the presence of extremely short bonds of metal-oxygen toward the interlayer alkali metals between the perovskite layers [17, 19]. Such shortness of the Ti-O distance leads to less interaction between the sodium atoms of the interlayer and the apex oxygen atoms of the perovskite layers. Therefore, these structural features may be a cause for ion-exchange reaction with other monovalent ions. Actually, the sodium ions in parent compounds are readily exchanged with silver and lithium ions in molten $AgNO_3$ and $LiNO_3$ to give novel layered oxides.

The ion-exchange compounds, $AgLnTiO_4$ and $LiLnTiO_4$ (Ln = La and Eu), are obtained in the form of well-cristallized powders, dark gray for the silver compounds and light-brownish white for the lithium compounds. The XRD study of $AgLaTiO_4$ and $LiLaTiO_4$ showed a tetragonal symmetry with only one systematic absence of $h + k = 2n + 1$ for hk0 reflections, indicating possible space groups P4/n or P4/nmm. On the other hand, reflection conditions of $AgEuTiO_4$ and $LiEuTiO_4$ are $k = 2n$ for 0kl and 0k0 reflections and $l = 2n$ for h0l and 00l reflections on the basis of an

orthorhombic symmetry. The possible space groups are Pbcm or $Pbc2_1$. These reflection conditions show the crystal symmetry which is the same as that of the parent compounds, $NaLaTiO_4$ and $NaEuTiO_4$. Despite of the considerable difference in ionic radii between the alkali ions and rare earth ions, the symmetry of the ion-exchage compounds is practically unchanged. From the previous chapters, it is found that the tilting of TiO_6 octahedra is caused by the mismatch between TiO_2 and LnO_2 layers. The replacement of sodium by silver and lithium in $NaLnTiO_4$ has shown the predominant role of the lanthanide in structural properties of these materials.

The Rietveld refinements for the ion-exchange compounds were, therefore, performed assuming the same structural model as that of the parent compounds. Initial atomic positions were calculated by modifying the coordinates of the parent compounds. In the early refinement stage of ion-exchange compounds, the site assignment for silver and lithium ions were not included. In final refinement stage, the location of the silver ion site was determined by difference Fourier maps. However, it was not possible to locate the remaining lithium atoms from the difference Fourier maps because of its low atomic scattering factor. Therefore, several trial models were fitted to the profiles using Rietveld program RIETAN. The small size of the Li^+ ion leads to a large contraction along the c-axis between perovskite layers. The spacing between the adjacent perovskite layers in both lithium compounds are about 0.14nm. This interlayer distance is too small to allow the lithium ions to be rock-salt coordination. In addition, the nine-fold coordination of lithium atom is unkown. The anomalously shortened lattice parameters obtained may be due to a coordination change for lithium atom, which is possibly in a four-fold

coordinate site. The refinements assuming four-fold coordinate site of lithium atoms converged to R_{wp} = 15.60% for $LiLaTiO_4$ and 15.15% for $LiEuTiO_4$. These relatively high R-factors are probably due to poor crystallinity occurring during the ion-exchange reaction. It is difficult to determine the accurate positions of lithium atom in between the perovskite layers, owing to the fact that lithium atom has a smaller contribution to the structure factors because of their small atomic scattering factors. Therefore, it is evident that the results obtained here for the atomic positions may be considered as a structural model rather than accurate structure. Although the silver ion-exchanged compounds give slightly poor crystallinity compared with the parent compounds, R-factors were reasonably converged due to relatively high atomic scattering factor of silver atom.

The results of the pattern fitting for $AgLnTiO_4$ and $LiLnTiO_4$ (Ln = La and Eu) are shown in Figs. 5.1 - 5.4. The crystallographic data finally obtained from Rietveld refinement are listed in Table 5.1 and 5.2. The structural models for $AgLnTiO_4$ and $LiLnTiO_4$ (Ln = La and Eu) are illustrated in Fig. 5.5 and 5.6, respectively. $AgLaTiO_4$ and $AgEuTiO_4$, which are prepared by the ion exchange reaction, retain the structural property of the parent compounds, $NaLaTiO_4$ and $NaEuTiO_4$. For example, the silver ion-exchanged compound, $AgEuTiO_4$, also show the deviation of titanium ions toward the silver ions and the tilts of the TiO_6 octahedra, leading to an orthorhombic structure. The silver ion-exchanged compounds, $AgLnTiO_4$ (Ln = La, Eu), consist of intergrowths of the perovskite sheets with the single layers of LnO and AgO with a distorted rock-salt coordination. The rock-salt type coordination of AgO found in $AgLnTiO_4$ is extremely rare in the normal oxides containing silver atoms [17]. In many cases, silver atoms

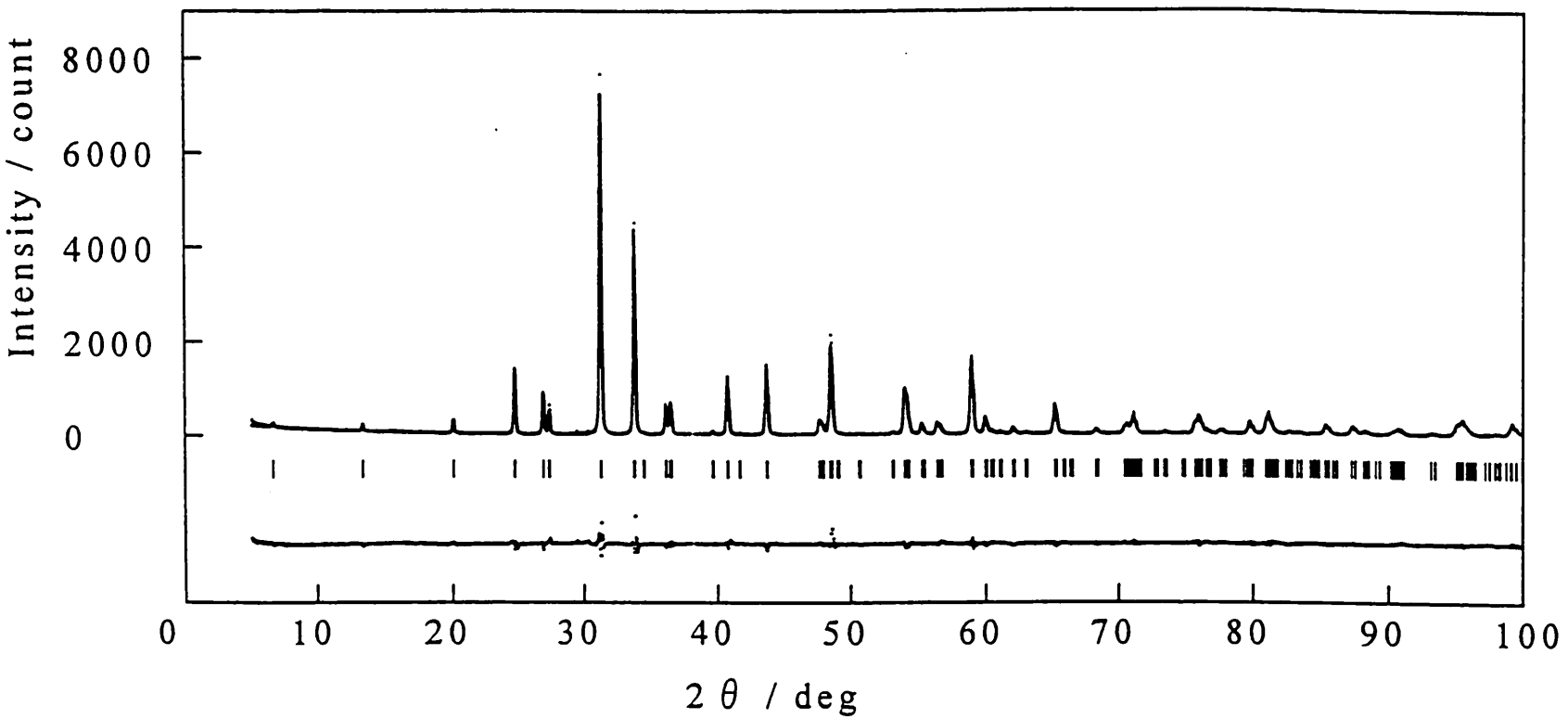

Fig. 5.1 X-ray powder pattern fitting for $AgLaTiO_4$. The calculated and observed patterns are shown on the top solid line and the dots, respectively. The vertical marks in the middle show positions calculated for Bragg reflections. The trace on the bottom is a plot of the difference between calculated and observed intensities.

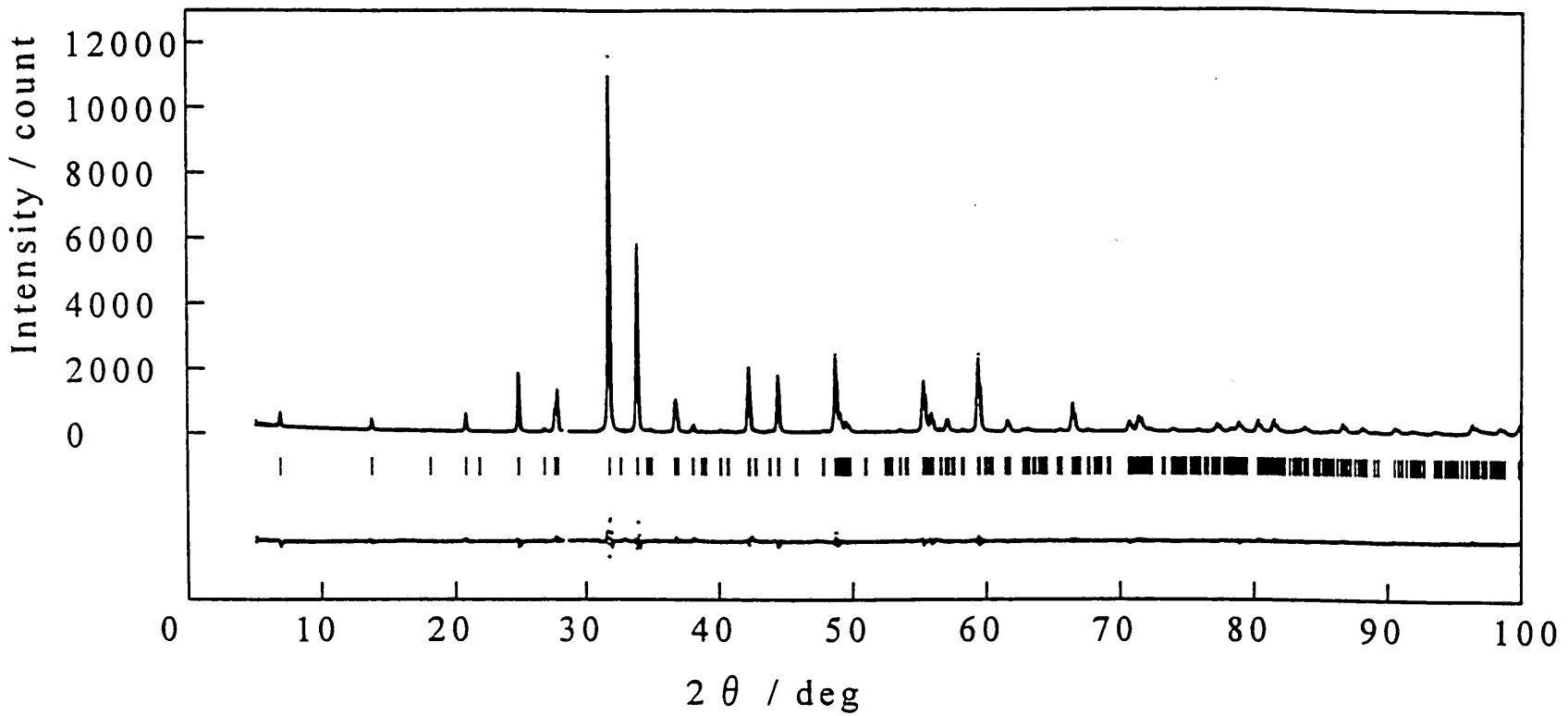

Fig. 5.2 X-ray powder pattern fitting for $AgEuTiO_4$.

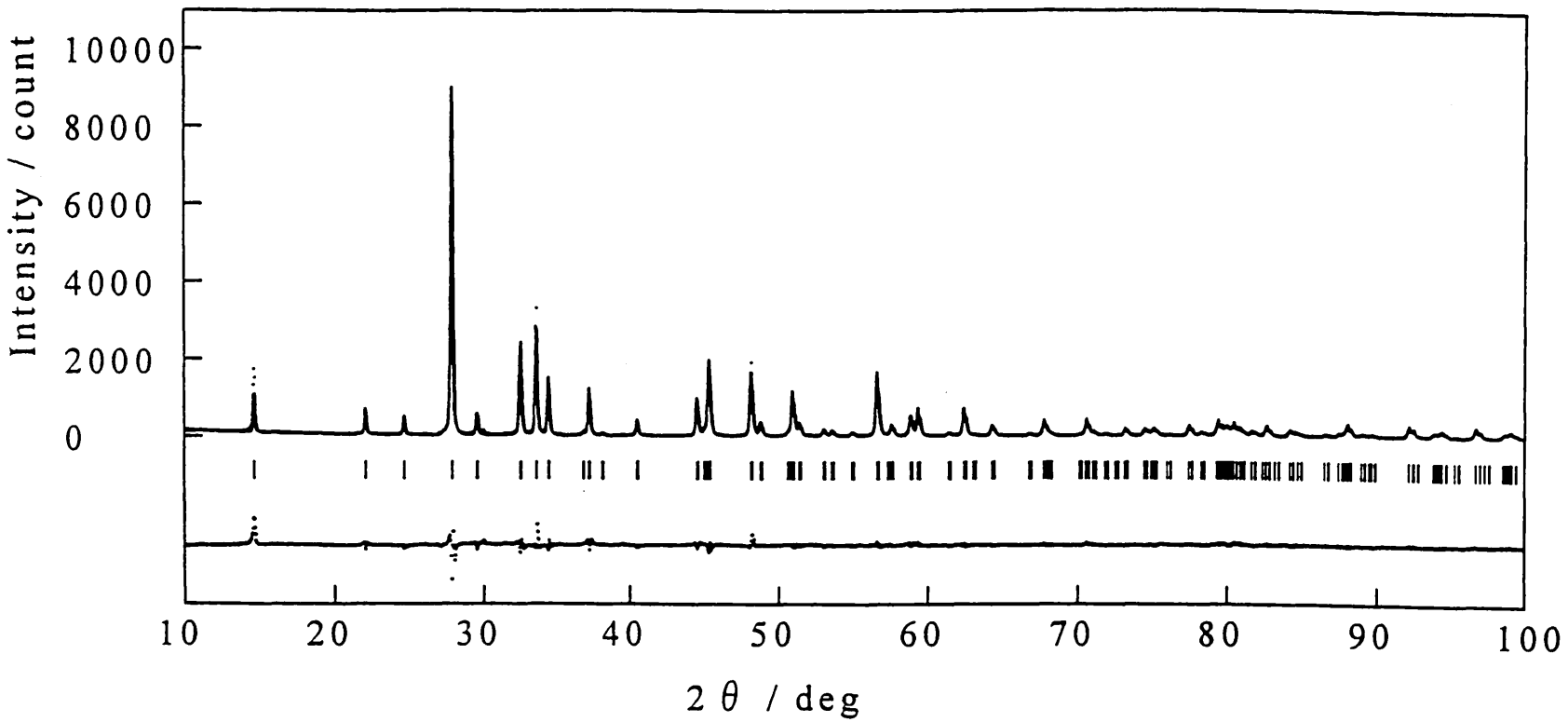

Fig. 5.3 X-ray powder pattern fitting for $LiLaTiO_4$.

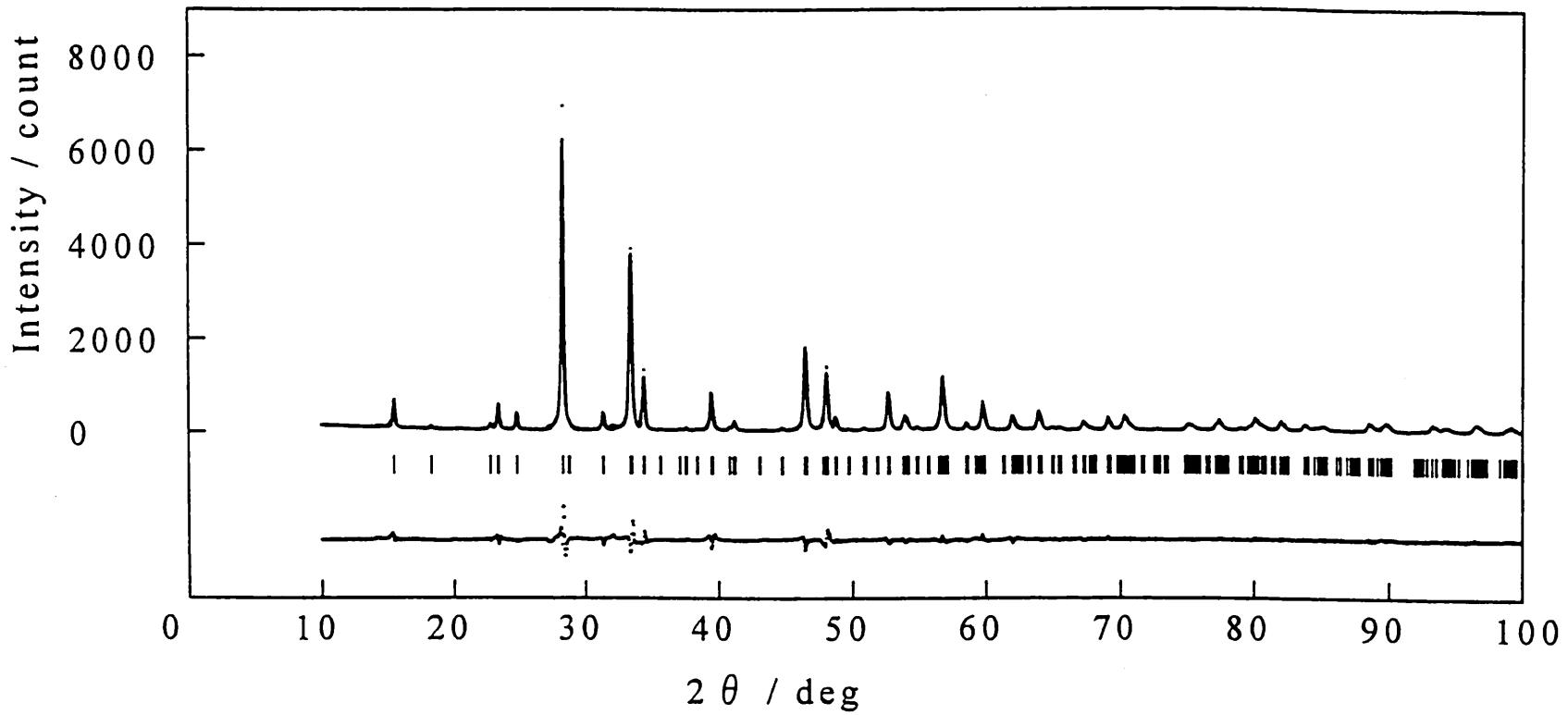

Fig. 5.4 X-ray powder pattern fitting for $LiEuTiO_4$.

Table 5.1 Crystallographic data for $AgLaTiO_4$ and $LiLaTiO_4$.

Sample	Atom	Site[a)]	x	y	z
$AgLaTiO_4$	Ag	2c	0.0	0.5	0.5806(5)
P4/nmm (No. 129)	La	2c	0.0	0.5	0.8908(4)
a = 0.37472(1)nm	Ti(1)	2c	0.0	0.5	0.276(1)
c = 1.32755(5)nm	O(1)	4f	0.0	0.0	0.241(3)
R_{wp} = 12.42%	O(2)	2c	0.0	0.5	0.077(3)
R_F = 2.35%	O(3)	2c	0.0	0.5	0.404(3)
$LiLaTiO_4$	Li	2a	0.0	0.0	0.0
P4/nmm (No. 129)	La	2c	0.0	0.5	0.3799(4)
a = 0.37696(1)nm	Ti(1)	2c	0.0	0.5	0.795(1)
c = 1.20625(5)nm	O(1)	4f	0.0	0.0	0.759(2)
R_{wp} = 15.60%	O(2)	2c	0.0	0.5	0.586(3)
R_F = 3.78%	O(3)	2c	0.0	0.5	0.937(3)

a) Multiplicity and Wyckoff notation.

Table 5.2 Crystallographic data for $AgEuTiO_4$ and $LiEuTiO_4$.

Sample	Atom	Site[a)]	x	y	z	B / nm^2
$AgEuTiO_4$	Ag	4d	0.5809(3)	0.0254(12)	0.25	0.010(1)
Pbcm (No. 57)	Eu	4d	0.8940(2)	0.0094(12)	0.25	0.004(1)
a = 1.28284(3)nm	Ti(1)	4d	0.2662(6)	0.0104(28)	0.25	0.005
b = 0.52815(6)nm	O(1)	4c	0.2345(36)	0.25	0.0	0.016(9)
c = 0.52820(6)nm	O(2)	4c	0.7717(33)	0.25	0.0	0.005
R_{wp} = 11.01%	O(3)	4d	0.0750(22)	0.0266(91)	0.25	0.028(10)
R_F = 2.58%	O(4)	4d	0.3986(22)	0.007(10)	0.25	0.028(9)
$LiEuTiO_4$	Li	4c	0.50(2)	0.25	0.0	0.005
Pbcm (No. 57)	Eu	4d	0.8816(4)	0.0198(11)	0.25	0.004(1)
a = 1.14066(6)nm	Ti(1)	4d	0.2885(10)	0.0083(42)	0.25	0.005
b = 0.5351(1)nm	O(1)	4c	0.2387(44)	0.25	0.0	0.02(2)
c = 0.5351(1)nm	O(2)	4c	0.7410(41)	0.25	0.0	0.01(2)
R_{wp} = 15.15%	O(3)	4d	0.0782(35)	-0.061(10)	0.25	0.03(1)
R_F = 3.16%	O(4)	4d	0.4343(28)	0.019(14)	0.25	0.005

a) Multiplicity and Wyckoff notation.

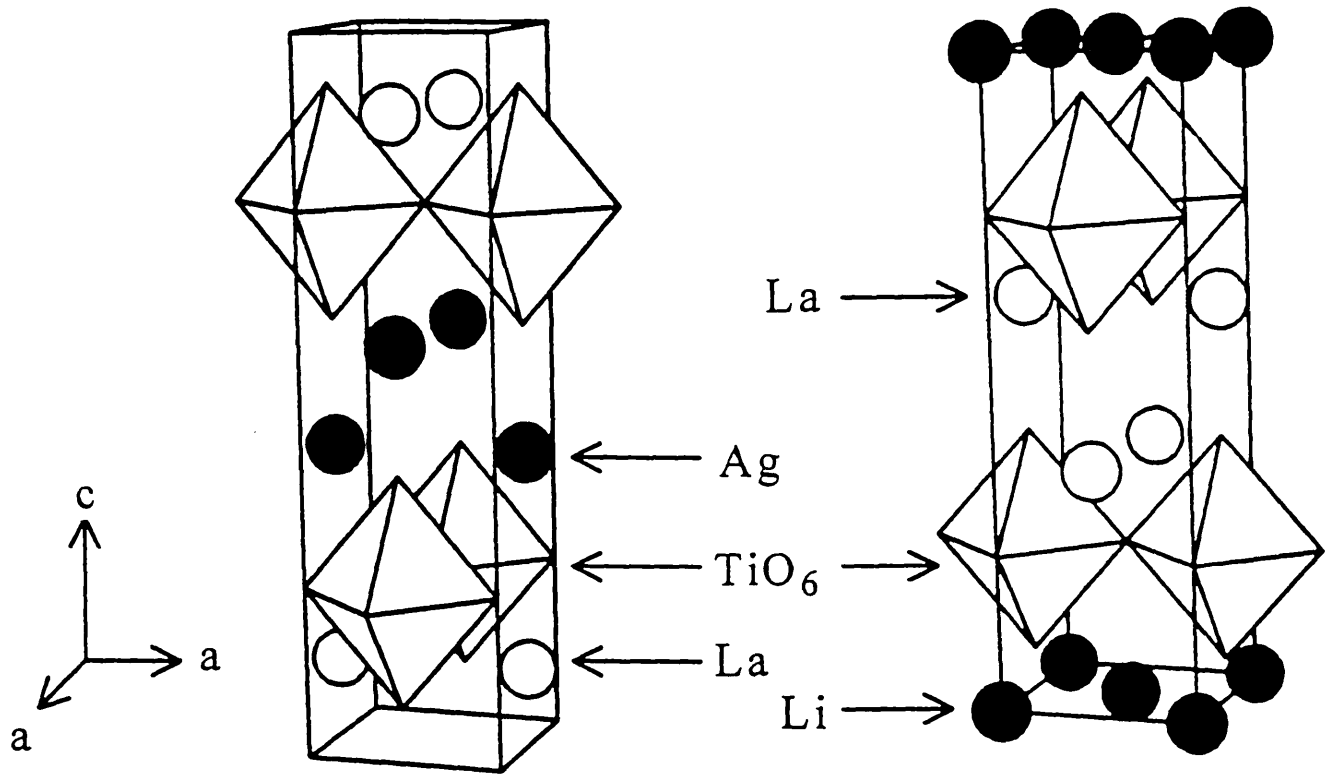

Fig. 5.5 Structural models of $AgLaTiO_4$ and $LiLaTiO_4$.

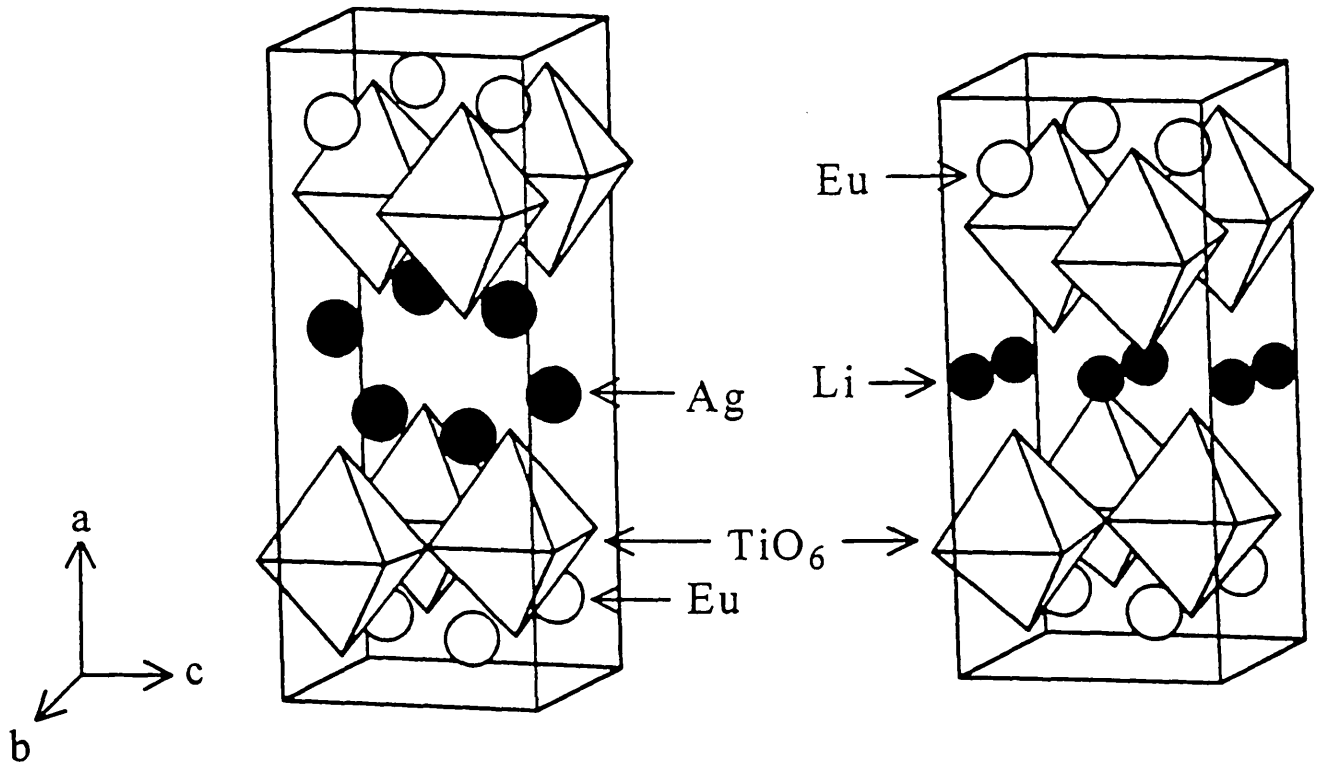

Fig. 5.6 Structural models of $AgEuTiO_4$ and $LiEuTiO_4$.

have a covalent bond character in oxide due to its electronic configuration. In such silver oxides, the distance of Ag-O bond is usually in the range 0.207 - 0.218nm for monovalent Ag ions [27, 28]. On the other hand, the distances of the Ag-O bond in $AgEuTiO_4$ are relatively large (ranging from 0.234(3) to 0.2660(5)nm), comparable with those found in $NaAgMoO_4$ (ranging from 0.225 to 0.255nm) [42]. Therefore, it seems that the silver atoms in the silver ion-exchanged compounds, $AgLaTiO_4$ and $AgEuTiO_4$, have an ionic bond character. In contrast, the coordination of Li-O found in $LiLaTiO_4$ and $LiEuTiO_4$ is not a rock-salt type. The lithium ions in both compounds have a tetrahedral coordination. The environment of the lithium ions in $LiEuTiO_4$ is illustrated in Fig. 5.7. For $LiEuTiO_4$, the Li-O distances in a LiO_4 tetrahedron are 0.195(8)nm and 0.212(8)nm. These bond distances are similar to those observed for the corresponding niobium compound, $Li_{1+x}LaNb_2O_7$ [43]. It seem likely that the LiO_4 tetrahedron in $LiEuTiO_4$ is fairly distorted from an ideal tetrahedron, because of too small ionic radius and high charge density of lithium layer. It is difficult to obtain the accurate information of lithium atom from powder XRD pattern analysis. Another approach, for example, neutron diffraction pattern analysis, is necessary to give a full structural description of this material.

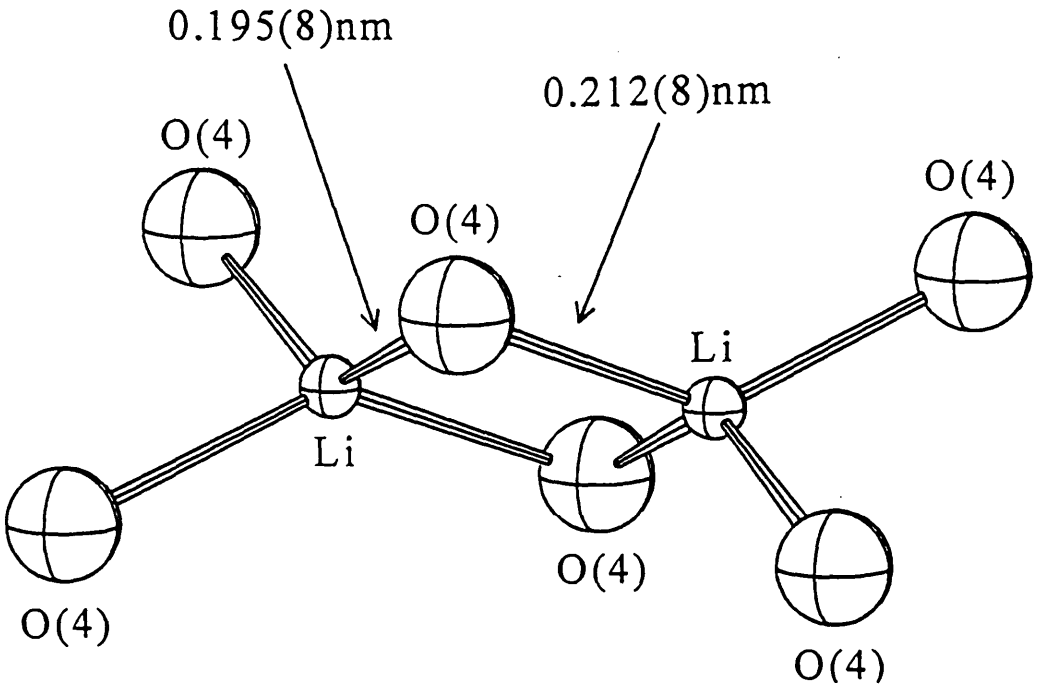

Fig. 5.7 Environment aroud lithium atoms in $LiEuTiO_4$.

5.4 Summary

Novel compounds, $AgEuTiO_4$ and $LiEuTiO_4$, have been synthesized by an ion-exchange reaction from parent compound, $NaEuTiO_4$. The crystal structure of $AgEuTiO_4$ and $LiEuTiO_4$ were determined by the powder XRD pattern. The silver ion-exchanged compound, $AgEuTiO_4$, retains the structural characteristics of the parent phase, $NaEuTiO_4$. On the other hand, the lithium ion in $LiEuTiO_4$, has a tetrahedral coordination because of too small ionic radius. These compounds, which are probably metastable, could only be obtained by the ion-exchange reaction.

Chapter 6

Luminescence Properties of Layered Perovskites activated by Eu^{3+} ions.

6.1 Introduction

Many compounds containing rare earth ions are very useful for phosphors and laser materials because rare earth ions can become an efficient luminescence center [44]. The emission is often quenched by doping rare earth ions over an critical concentration [45, 46]. This phenomenon is called "concentration quenching". It is well known that the interaction between rare earth ions results in the concentration quenching, but there are a number of unclarified discussions regarding the nature of the interaction. Although the concentration quenching is strongly dependent on the structural dimensionality of the host material, investigations on the luminescence properties of low-dimensional compounds are rather fewer than those on three-dimensional compounds [47 - 49]. In addition, these studies have not been carried out systematically.

In this chapter, the relationship between structural arrangement of rare earth ions and the concentration quenching of the luminescence in layered perovskite compounds of $Na_2Gd_{2x}Eu_{2(1-x)}Ti_3O_{10}$ with a triple perovskite layer and $NaGd_xEu_{1-x}TiO_4$ with a single perovskite layer are investigated. The crystal structure of $Na_2Eu_2Ti_3O_{10}$ remains still unknown although prototype structure model is presumed [12]. Therefore, the crystal structure of this compound was determined by the Rietveld analysis for

powder XRD data. The difference in the critical concentration for the concentration quenching observed in both compounds is discussed on the basis of the determined crystal structure.

6.2 Experimental

$Na_2Gd_{2x}Eu_{2(1-x)}Ti_3O_{10}$ and $NaGd_xEu_{1-x}TiO_4$ were prepared as described in chapter 3 and 4. XRD patterns were recorded on a Rigaku RAD-rA diffractometer, using Cu-K α radiation which was monochromatized by a curved crystal of graphite. The data were collected on thoroughly ground powders by a step-scanning mode in the 2 θ range of 5 - 100° with a step width of 0.02° and a step time of 4s. The indexing of the powder XRD pattern for these compounds was examined with the aid of computer program CELL [24]. Data analysis for the structural refinement was carried out by the Rietveld method, using the RIETAN profile refinement program [25] on an ACOS2010 computer at Niigata University.

Phase purity of these compounds was examined by the energy-dispersive X-ray (EDX) method using an electron microscope (ABT EM002B) equipped with an EDX analyzer. Excitation and emission spectra were measured on a powder sample using a Shimadzu RF-5000 spectrophotofluorometer.

6.3 Results and Discussion

Space group of $Na_2Ln_2Ti_3O_{10}$ (Ln = rare earths) has not been found. Gondrand and Joubert [12] reported the synthesis of a series of $Na_2Ln_2Ti_3O_{10}$ (Ln = La, Nd, Eu, Gd). From the electron diffraction analysis, they suggested that $Na_2Gd_2Ti_3O_{10}$ crystallizes in an orthorhombic system with $a \fallingdotseq b \fallingdotseq 0.770$nm and $c \fallingdotseq 2.84$nm. They also pointed out that the structure of these compounds is analogous to that of the Ruddlesden-Popper type compound, $Sr_4Ti_3O_{10}$, with a triple perovskite layer because of the a and b lattice parameters nearly equal to the values as twice large as those of the Ruddlesden-Popper compound with I4/mmm space group. We also observed weak electron diffraction spots corresponding to the doubling of a and b lattice parameters for $Na_2Eu_2Ti_3O_{10}$. According to the group theoretical analysis of space group by Hatch et al. [50], we tried to determine the possible space group for $Na_2Eu_2Ti_3O_{10}$. However, the Rietveld analysis using the several space groups expected from the group theory gave no reasonable solution with physically meaningful structural parameters. This type of superstructure of $Na_2Eu_2Ti_3O_{10}$ is probably related to an only slight displacement of oxygen atoms, as observed in $BaNdMnO_4$ [51]. Therefore, we carried out the Rietveld analysis based on the space group I4/mmm (Z = 2). It should be noted that the results in the present structural determination express an averaged structure for $Na_2Eu_2Ti_3O_{10}$.

The results of the pattern fitting for $Na_2Eu_2Ti_3O_{10}$ is shown in Fig. 6.1. The crystallographic data finally obtained from the Rietveld refinement are listed in Tables 6.1. The structural models for $Na_2Eu_2Ti_3O_{10}$ and $NaEuTiO_4$ are illustrated in Figs. 6.2 and 6.3. These compounds exhibit an ordering of

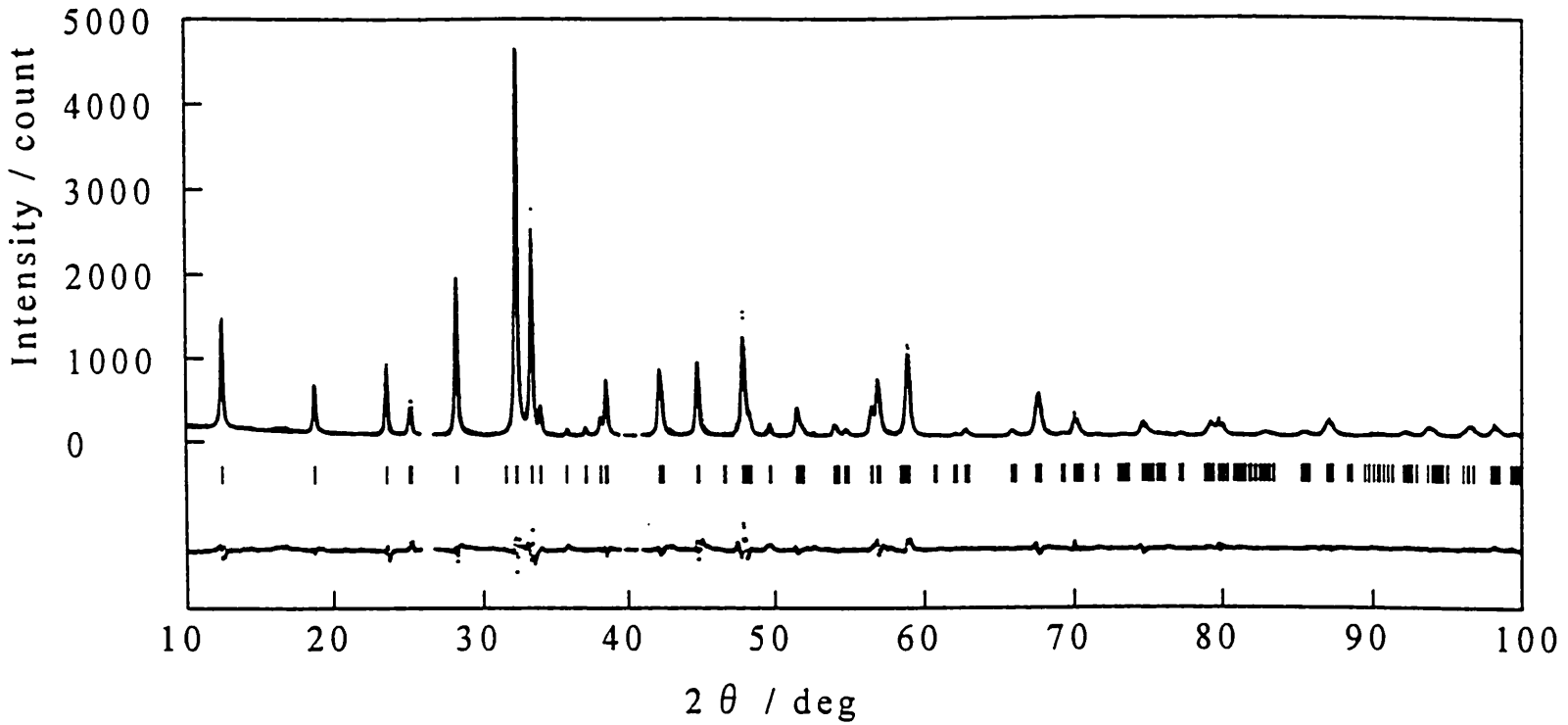

Fig. 6.1 X-ray powder pattern fitting for $Na_2Eu_2Ti_3O_{10}$. The calculated and observed patterns are shown on the top solid line and the dots, respectively. The vertical marks in the middle show positions calculated for Bragg reflections. The trace on the bottom is a plot of the difference between calculated and observed intensities.

Table 6.1 Crystallographic data for $Na_2Eu_2Ti_3O_{10}$.

Space group	I4/mmm (No. 139)
Lattice constant / nm	a = 0.37956(2), c = 2.8280(1)
Reliability factors	R_{wp} = 0.1132, R_p = 0.0870, R_E = 0.0783, R_I = 0.0400, R_F = 0.0202

Atom	Site[a)]	x	y	z	B / nm^2
Na	4e	0.0	0.0	0.2882(10)	0.0004(77)
Eu	4e	0.0	0.0	0.4241(2)	0.012(2)
Ti(1)	2a	0.0	0.0	0.0	0.005
Ti(2)	4e	0.0	0.0	0.1478(5)	0.005
O(1)	4c	0.0	0.5	0.0	0.11(3)
O(2)	4e	0.0	0.0	0.0635(22)	0.065(20)
O(3)	4e	0.0	0.0	0.2076(16)	0.020(13)
O(4)	8g	0.0	0.5	0.1331(12)	0.025(11)

a) Multiplicity and Wyckoff notation.

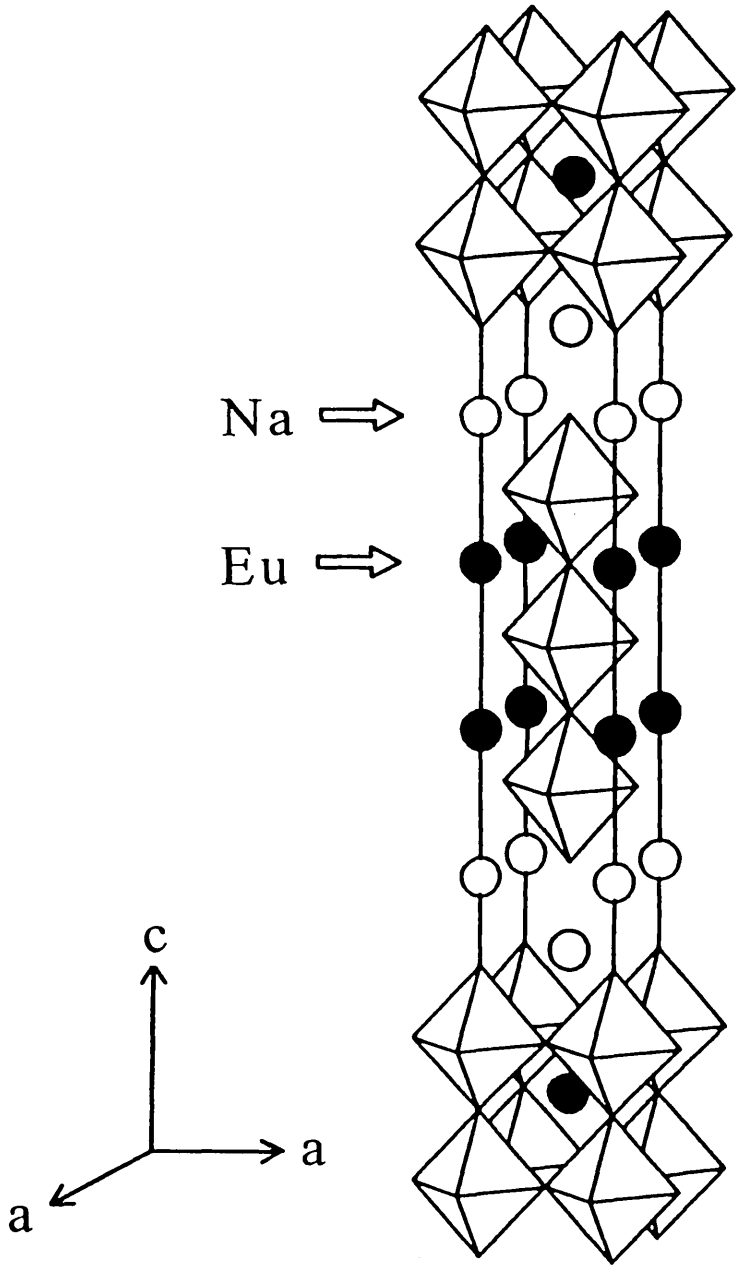

Fig. 6.2 Structural model of $Na_2Eu_2Ti_3O_{10}$.

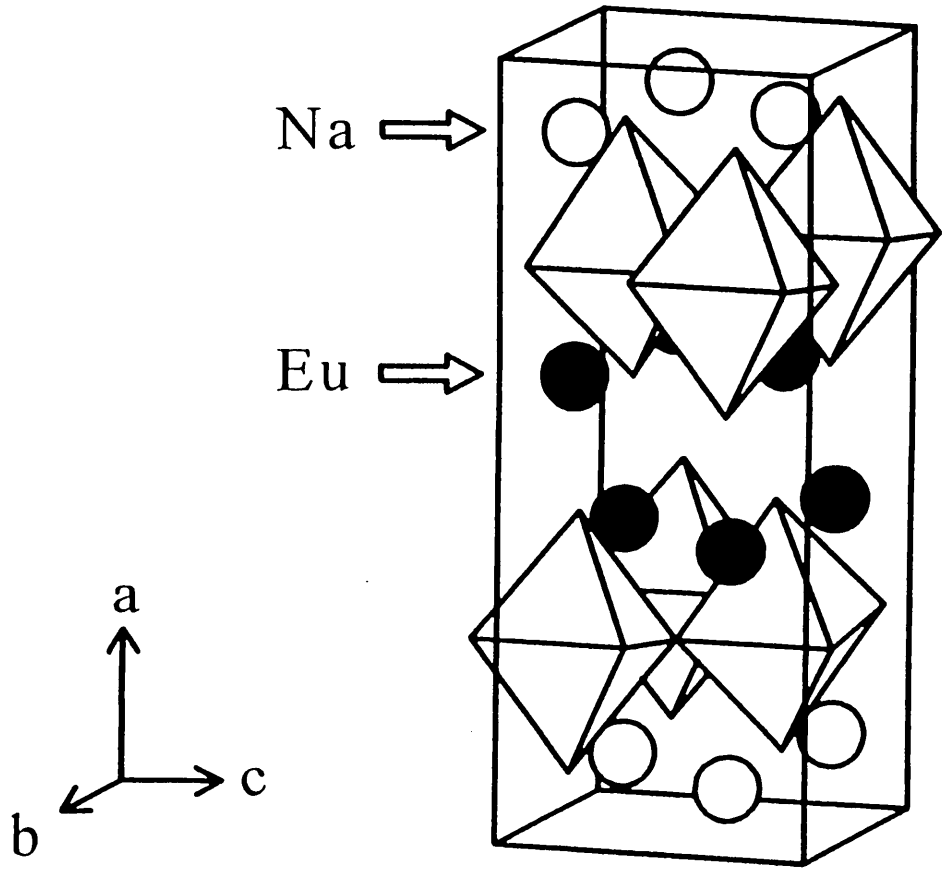

Fig. 6.3 Structural model of $NaEuTiO_4$.

the cations in the form [-Eu-Eu-Na-Na-]. The Eu^{3+} ions occupy only one crystallographic site and form a quasi-two-dimensional plane consisting of a double layer perpendicular to the c-axis in $Na_2Eu_2Ti_3O_{10}$ and the a-axis in $NaEuTiO_4$. The shortest Eu^{3+} - Eu^{3+} distances (ca. 0.38nm in both compounds) within the quasi-two-dimensional plane are much shorter than those between the adjacent two planes (ca. 0.98nm in $Na_2Eu_2Ti_3O_{10}$ and ca. 1.25nm in $NaEuTiO_4$). The shortest Eu^{3+} - Eu^{3+} distances are about the same in both compounds. Therefore, these layered perovskite compounds can be a suitable system to investigate two-dimensional energy transfer among doped Eu^{3+} ions.

Figure 6.4 shows the emission spectra for $Na_2Gd_{2(1-x)}Eu_{2x}Ti_3O_{10}$ and $NaGd_{1-x}Eu_xTiO_4$ at 300K. The excitation wavelength is 401.6nm which is the optimum excitation wavelength for the strongest emission. The emission spectra show two strong lines, which correspond to the $^5D_0$ - $^7F_1$ and $^5D_0$ - $^7F_2$ transitions of Eu^{3+} [52]. Several weak emissions from higher ^5D levels were also observed in the range of 400 - 500nm for the cases with low concentrations of Eu^{3+} ions.

Figure 6.5 shows the dependence of the strongest $^5D_0$ - $^7F_2$ emission intensity on the Eu^{3+} concentration. The critical values for the concentration quenching are $x = 0.40$ for $Na_2Gd_{2(1-x)}Eu_{2x}Ti_3O_{10}$ and $x = 0.25$ for $NaGd_{1-x}Eu_xTiO_4$. The experimental value of the critical concentration for $NaGd_{1-x}Eu_xTiO_4$ is in good agreement with the result of Berdowski and Blasse [47, 53]. Although the Eu^{3+} - Eu^{3+} distances in these compounds are rather short, these values are much higher than those observed in conventional inorganic phosphors [54, 55]. The high critical values in the

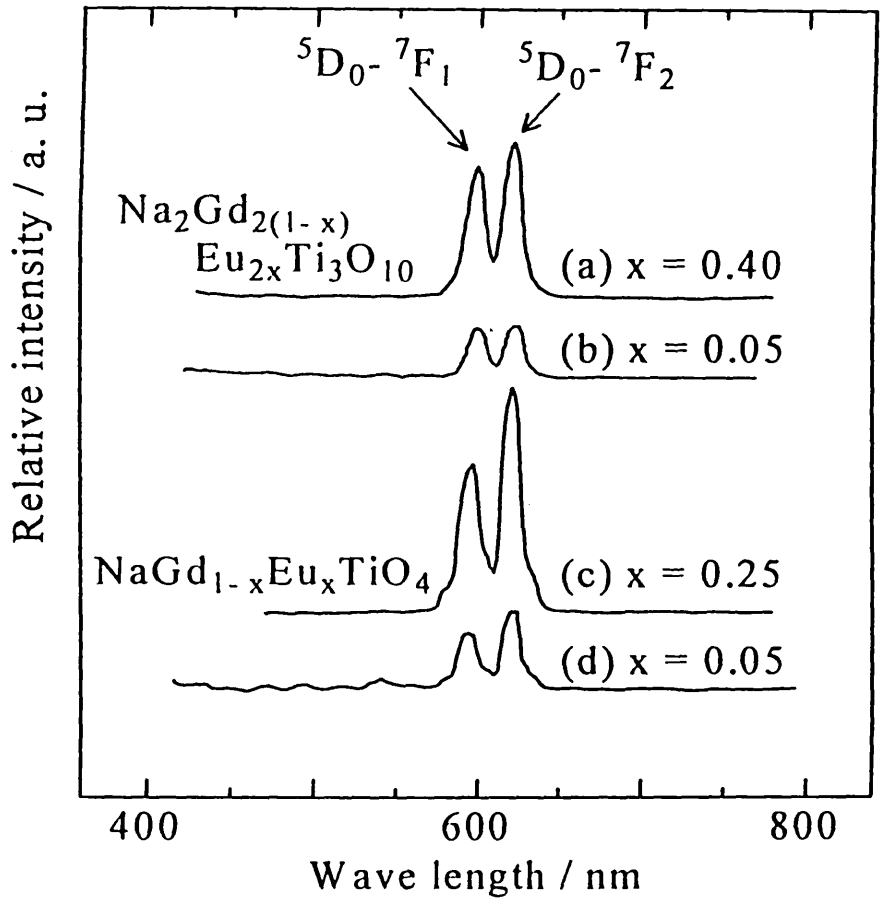

Fig. 6.4 Emission spectra of (a) $Na_2Gd_{1.2}Eu_{0.8}Ti_3O_{10}$, (b) $Na_2Gd_{1.9}Eu_{0.1}Ti_3O_{10}$, (c) $NaGd_{0.75}Eu_{0.25}TiO_4$ and (d) $NaGd_{0.95}Eu_{0.05}TiO_4$ at 300K with 401.6nm excitation.

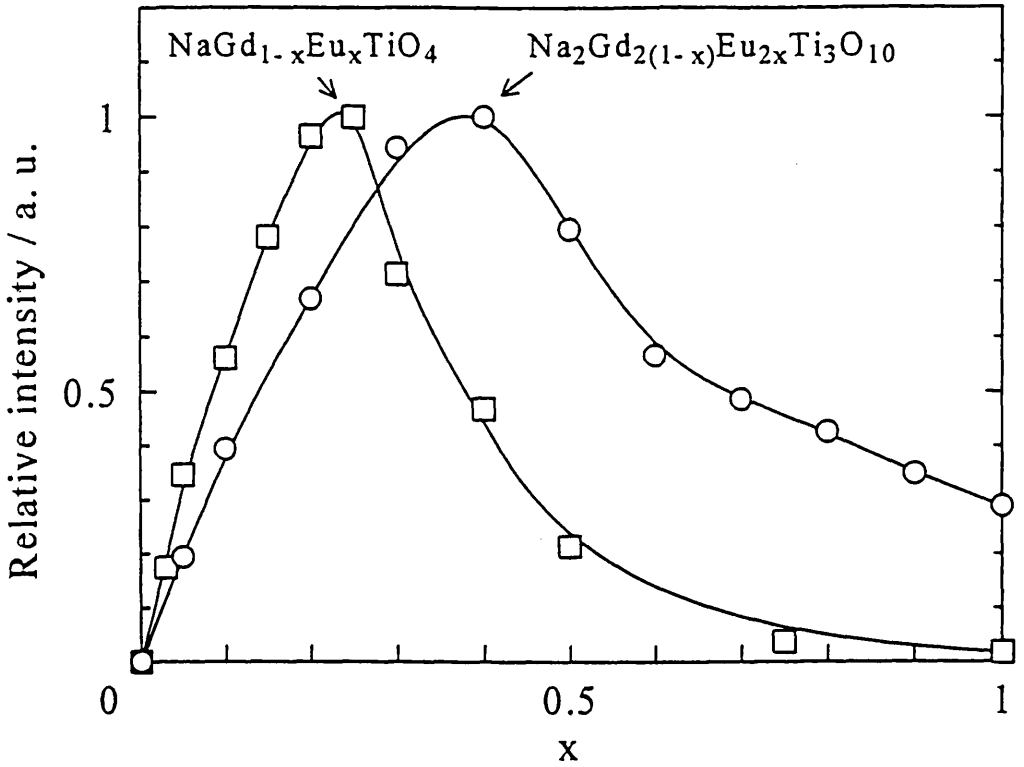

Fig. 6.5 The dependence of $^5D_0$ - $^7F_2$ emission intensity on Eu^{3+} concentration.

layered perovskite compounds indicate that the energy transfer is restricted to the quasi-two-dimensional Eu^{3+} sublattice.

The theoretical values of the critical concentrations in both compounds were determined by the following approximate expression using the percolation model [56, 57], because it is impossible to solve the problem analytically.

$$z \cdot P_c = d / (d - 1), \qquad (6 - 1)$$

where z is the coordination number, P_c the critical concentration and d the dimensionality for the percolation lattice. It should be noted that this expression gives only an approximate value. The computer simulations are now in progress to obtain the more accurate values. The percolation model can be applied to the given compounds based on the following two assumptions: i) the interaction among Eu^{3+} ions occurs only among the nearest sites, ii) the concentration quenching is due to the energy transfer from a percolation cluster of the nearly two dimensional Eu^{3+} sublattice to killer centers, e.g., unknown defects or a very small amount impurities acting as an acceptor.

Figure 6.6 shows the schematic representation of the local environment of Eu^{3+} ions. There are two kind of the distances among the adjacent Eu^{3+} - Eu^{3+} ions in $Na_2Eu_2Ti_3O_{10}$, i.e., one group is four short distances (0.37956(2)nm) and the other a long distance (0.429(1)nm). The distances for the adjacent Eu^{3+} ions for $NaEuTiO_4$ are classified into three types, i.e., two short distances (0.3630(4)nm), four moderate distances (0.3795(3)nm, 0.3800(3)nm), and two long distances (0.3911(4)nm). These

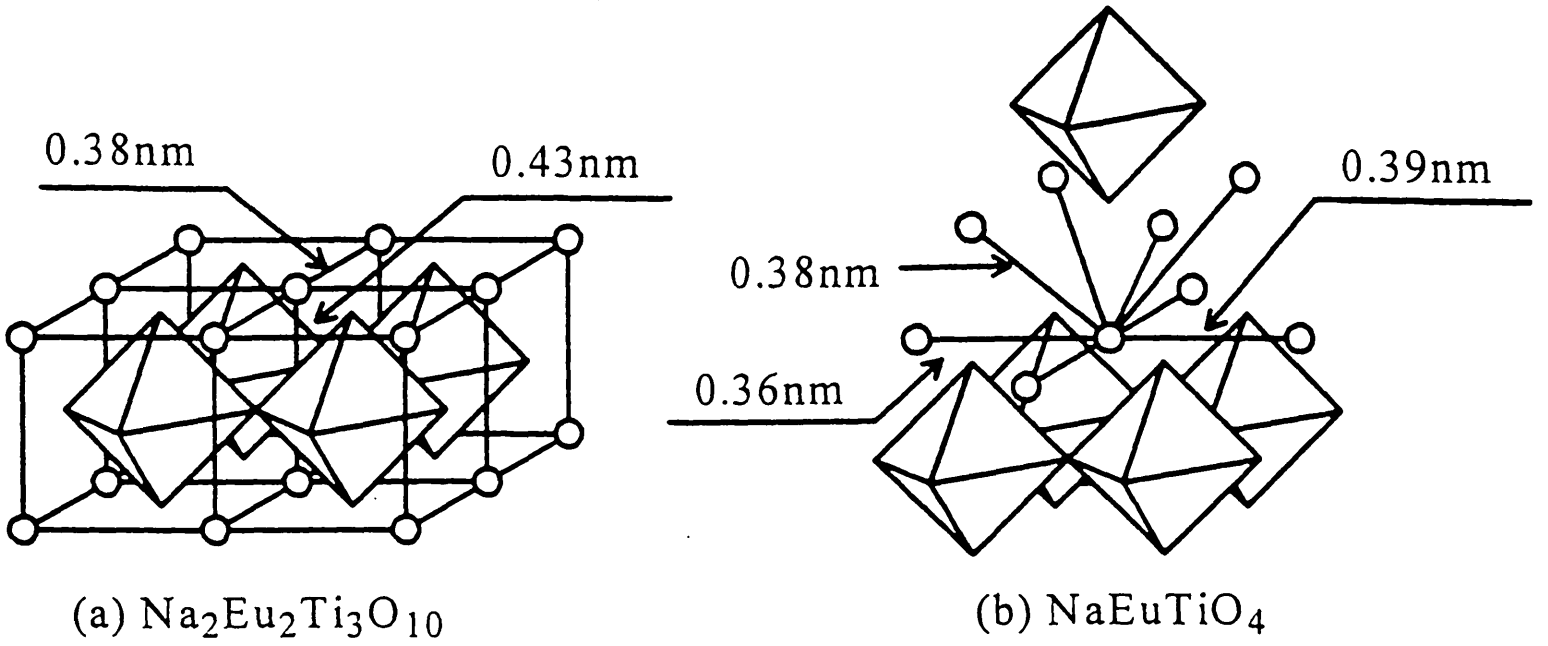

Fig. 6.6 Schematic representation of local environment of Eu^{3+} ions for $Na_2Eu_2Ti_3O_{10}$ and $NaEuTiO_4$. Eu^{3+} sites and TiO_6 octahedra are shown as an open circle and octahedra, respectively.

distances can be considered as nearly equal. Therefore, the coordination numbers are z = 5 for $Na_2Gd_{2(1-x)}Eu_{2x}Ti_3O_{10}$ and z = 8 for $NaGd_{1-x}Eu_xTiO_4$. Since the value of d can be taken as 2 owing to the layered structure, the critical concentration, P_c, determined by equation(1) are equal to x = 0.40 for $Na_2Gd_{2(1-x)}Eu_{2x}Ti_3O_{10}$ and x = 0.25 for $NaGd_{1-x}Eu_xTiO_4$. The experimental values agree well with the calculation results. This clearly indicates that the energy transfer occurs only within the nearest Eu^{3+} ions in both compounds.

Berdowski and Blasse [53] claim that the interaction between the Eu^{3+} ions in two-dimensional compounds is due to a super-exchange interaction. In this case, the super-exchange interaction is taken place by the spin exchange via O^{2-} anion. If the nature of the interaction for these compounds is the super-exchange, the interaction between the second nearest neighboring Eu^{3+} ions should also become important. The critical concentrations observed are too large on the basis of such a super-exchange mechanism only. Since the interaction occurs between the nearest sites, a direct interaction, i.e., multipole - multipole interaction, must be taken into account. Therefore, the interaction between Eu^{3+} ions in the layered perovskite compounds is considered to be due to multipole - multipole mechanism. Furthermore, such short critical distances of the interaction suggest that the mechanism of higher order multipole (dipole-quadrupole, quadrupole-quadrupole) is the dominant in the energy transfer between the Eu^{3+} ions in these compounds. These explanations can satisfactorily interpret the well known facts that the low-dimensional compounds have a high critical value of concentration quenching.

6.4 Summary

Dependence of the emission intensity on Eu^{3+} concentration in $Na_2Gd_{2(1-x)}Eu_{2x}Ti_3O_{10}$ with a triple perovskite layer and $NaGd_{1-x}Eu_xTiO_4$ with a single perovskite layer was studied. Critical values for the concentration quenching are x=0.40 for $Na_2Gd_{2(1-x)}Eu_{2x}Ti_3O_{10}$ and x=0.25 for $NaGd_{1-x}Eu_xTiO_4$. The difference of the critical concentration between both compounds is discussed in terms of their crystal structures determined by the powder XRD patterns using the Rietveld method. The concentration quenching found in these compounds can be explained by means of a percolation model with nearly two dimensional interactions between Eu^{3+} sites in the host lattice.

Chapter 7

Concluding Remarks

The relationship between crystal structure and two-dimensional physical properties in layered perovskite compounds have attracted much attention. In this thesis, low-dimensional electric conducting behavior and luminescence properties were studied. The results are discussed in terms of the crystal structures determined by the powder XRD patterns using Rietveld method. The knowledge obtained in this study will serve as a guide for designing new compounds of this structure. The results are summarized as follows:

1. Although the anhydrous $K_2La_2Ti_3O_{10}$ compound and newly prepared $Ag_2La_2Ti_3O_{10}$ compound, which are triple layered perovskites, have almost the same crystal structure, a drastic difference in the bond character of M-O (M = K, Ag) was observed between the two compounds, i.e., completely ionic character for the K-O bond and relatively strong covalent character for the Ag-O bond along the direction of the c axis. An almost pure ion conduction of silver was observed at the temperatures below 200℃, while the mixed conduction with silver ion transport number of 0.5 was observed over this temperature.

2. The ionic conductivity of $Na_2La_2Ti_3O_{10}$ was not very high compared with those of niobate compounds, $NaLaNb_2O_7$ and $NaCa_2NaNb_4O_{13}$. Such a low ionic conductivity is due to the rigid rock-salt-type coordination around sodium ions located at the interlayer.

3. The crystal structures of single layered perovskite compounds, $NaLnTiO_4$ (Ln = La, Eu, Gd, Y, and Lu), are determined. $NaLnTiO_4$ have a tetragonal symmetry for Ln = La, while an orthorhombic symmetry for Ln = Eu - Lu. The lowering of symmetry are discussed in terms of the mismatch between TiO_2 and LnO_2 layers. Using two parameters, c/a ratio and tolerance factor t, the change of symmetry of crystal structure can be explained. The lowering of symmetry are considered to be produced by the mismatch between TiO_2 and LnO_2 layers

4. New ion-exchanged compounds of $AgLnTiO_4$ and $LiLnTiO_4$ (Ln = La and Eu) are synthesized. Silver ion-exchanged compounds, $AgLnTiO_4$, retain the structural property of the parent phase, $NaLnTiO_4$. On the other hand, lithium ion in $LiLnTiO_4$, has a tetrahedral coordination because of too small ionic radius. These compounds, which are probably metastable, could only be obtained by ion-exchange reaction.

5. The critical concentrations for photoluminescence of $NaGdTiO_4$ and $Na_2Gd_2Ti_3O_{10}$ doped by Eu^{3+} are x=0.40 for $Na_2Gd_{2(1-x)}Eu_{2x}Ti_3O_{10}$ and x=0.25 for $NaGd_{1-x}Eu_xTiO_4$. The concentration quenching found in these compounds can be explained by means of a percolation model with nearly two dimensional interactions between Eu^{3+} sites in the host lattice.

References

1) J. F. Schooley, W. R. Hosler and M. L. Cohen, *Phys. Rev. Lett.*, 12, 474 (1964)

2) J. M. Bolts and M. S. Wrighton, *J. Phys. Chem.*, 80, 2641 (1976)

3) R. J. D. Tilley, *J. Solid State Chem.*, 21, 293 (1977)

4) H. H. Kung, H. S. Jarett, A. W. Sleight and A. Feretti, *J. Appl. Phys.*, 48, 2463 (1977)

5) K. Wakino, K. Minai and H. Tamura, *J. Am. Ceram. Soc.*, 67, 278 (1984)

6) K. A. Muller and W. Berlinger, *Phys. Rev. B* 34, 6130 (1986)

7) S. N. Ruddlesden and P. Popper, *Acta Crystallogr.*, 10, 538 (1957)

8) J. D. Bednorz and K. A. Muller, *Z. Phys. B* 64, 189 (1986)

9) P. Ganguly and C. N. R. Rao, *J. Solid State Chem.*, 53, 193 (1984)

10) R. A. Mohan Ram, L. Ganapathi, P. Ganguly, and C. N. R. Rao, *J. Solid State Chem.*, 63, 139 (1986)

11) H. Ikeda, K. Iwasa and K. H. Andersen, *J. Phys. Soc. Japan*, 62, 3832 (1993)

12) M. Gondrand and J. C. Joubert, *Rev. Chim. Miner.*, 24, 33 (1987)

13) J. Gopalakrishnan and V. Bhat, *Inorg. Chem.*, 26, 4299 (1987)

14) M. Dion, M. Ganne and M. Tournoux, *Mater.Res.Bull.*,16, 1429 (1981)

15) A. J. Jacobson, J. T. Lewandowski and J. W. Johnson, *J. Less Common Met.*, 116, 137 (1986)

16) G. Okada, S. Ohmiya, S. Matsushima and K. Kobayashi, *Denki Kagaku*, 60, 336 (1992)

17) M. Sato, K. Toda, J. Watanabe and K.Uematsu, *Nippon Kagaku Kaishi*, 640 (1993)

18) M. Sato, J. Watanabe and K. Uematsu, *J. Solid State Chem.*, 107, 460 (1993)

19) M. Sato, J. Abo and T. Jin, *Solid State Ionics*, 57, 285 (1992)

20) M. Sato, Y. Kono and T. Jin, *J. Ceram. Soc. Japan*, 101, 980 (1993)

21) M. Sato, J. Abo, T. Jin and M. Ohta, *J. Alloys Comp.*, 192, 81 (1993)

22) K. Domen, J. Yoshimura, T. Sekine, A. Tanaka and T. Onishi, *Catal. Lett.*, 4, 339, (1990)

23) M. Vallino, *Atti Accad. Sci. Torino, Cl. Sci. Fis., Mat. Nat.*, 117, 85 (1985)

24) Y. Takaki, T. Taniguchi, H. Yamaguchi and T. Ogura, *J. Ceram. Soc. Japan. Inter. Ed.*, 95, 565 (1987)

25) F. Izumi, *Nippon Kesshou Gakkaishi*, 27, 23 (1985)

26) R. D. Shannon, *Acta Crystallogr. Sect A*32, 751 (1976)

27) V. H. Hahn and C. D. Lorenz, *Z. Anorg. Allg. Chem.*, 290 ,68 (1957)

28) S. Okamoto, S. I. Okamoto and T. Ito, *Acta Crystallogr. Sect B*28, 1774 (1972)

29) P. C. Allen and D. Lazarus, *Phys. Rev. B*17, 1913 (1978)

30) B. B. Owens and G. R. Argue, *J. Electrochem. Soc.*, 117, 898 (1970)

31) M. Abe and K. Uchino, *Mater. Res. Bull.*, 9, 147 (1974)

32) G. Blasse, *J. Inorg. Nucl. Chem.*, 30, 656 (1968)

33) S. N. Ruddlesden and P. Popper, *Acta Crystallogr.*, 11, 54 (1958)

34) K. R. Udayakumar and A. N. Cormack, *J. Am. Ceram. Soc.*, 71, 469 (1988)

35) M. Fujimoto, J. Tanaka and S. Shirasaki, *Jpn. J. Appl. Phys.*, 27, 1162 (1988)

36) R. J. Cava, J. J. Krajewskim W. F. Peck Jr, B. Batlogg, L. W. Rupp Jr, R. M. Fleming, A. C. W. P. James and P. Marsh, *Nature*, 338, 328 (1989)

37) G. Blasse and G. P. M. Van Den Heuvel, *J. Solid State Chem.*, 10, 206 (1974)

38) C. Linares and M. Blanchard, *C. R. Acad. Sc. Paris, t.* 286, *Serie B*, 387 (1978)

39) M. M. Elcombe, E. H. Kisi, K. D. Hawkins, T. J. White, P. Goodman and S. Matheson, *Acta Crystallogr. Sect B*, 47, 305 (1991)

40) K. Toda, Y.Kameo, M.Ohta and M. Sato, *J. Alloys Comp.*, submitted for publication.

41) K. Toda, Y. Kameo, M. Ohta and M. Sato, *J. Ceram. Soc. Japan*, 102, 737 (1994)

42) A. Rulmond, P. Tarte, G. Foumakoya, A. M. Fransolet and J. Choisnet, *J. Solid State Chem.*, 76, 18 (1988)

43) M. Sato, T. Jin and H. Ueda, *Chem. Lett.*, 161 (1994)

44) G. Blasse, *J. Alloys Comp.*, 192, 17 (1993)

45) L. G. Van Uitert, R. C. Linares, R. R. Soden, and A. A. Ballman, *J.Chem.Phys.*, 36, 702 (1962)

46) L. G. Van Uitert and S. Iida, *J. Chem. Phys.*, 37, 986 (1962)

47) P. A. M. Berdowski and G. Blasse, *J. Lumin.*, 29, 243 (1984)

48) F. W. Tian, C. Fouassier and P. Hagenmuller, *J. Phys. Chem. Solids*, 48, 245 (1987)

49) T. Endo, A. Shibuya, H. Takizawa and M. Shimada, *J. Alloys Comp.*, 192, 50 (1993)

50) D. M. Hatch, H. T. Stokes, K. S. Aleksandrov and S. V. Misyul, *Phys. Rev. B*, 39, 9282 (1989)

51) N. Kamegashira, S. Ueno, H. Saito-Nakano and K. Enami, *Mat. Res. Bull.*, 29, 185 (1994)

52) G. Blasse, in K. A. Gschneidner, Jr., and L. Eyring (eds.), *Handbook on the Physics and Chemistry of Rare Earths*, North-Hollandm Amsterdam, 1979, p. 237

53) P. A. M. Berdowski and G. Blasse, *J. Solid State Chem.*, 63, 86 (1986)

54) A. J. De Vries, J. P. M. Van Vliet and G. Blasse, *Phys. Status Soldi B*, 149, 391 (1988)

55) T. Endo, T. Masuda, H. Takizawa and M. Shimada, *J. Mat. Sci. Lett.*, 11, 1330 (1992)

56) C. Domb and M. F. Sykes, *Phys. Rev.*, 122, 77 (1961)

57) V. A. Vyssotsky, S. B. Gordon, H. L. Frisch and J. M. Hammersley, *Phys. Rev.*, 123, 1566 (1961)

ACKNOWLEDGMENT

The author would like to thank Professor Mineo Sato, Professor Koji Isogai and Professor Yoshio Masuda, at the Graduate School of Science and Technology, Niigata University for their continuous guidance and encouragement.

The author would also like to thank Professor Koichi Kato, Professor Hiroshi Miyamoto, Associate Professor Yoshie Kitayama and Associate Professor Masatoshi Ohta for their kind informative suggestions in this thesis.

The author is greatly indebted to Mr. Kazuyoshi Uematsu for his helpful advice and heartful encouragement.

The author also thanks the co-worker, Mr. Jun Watanabe, Mr. Yutaka Kameo and Mr. Satoru Kurita for their assistance, and Mr. Yasuhisa Kono, Mr. Yoshiki Hama, Mr. Hirokazu Ueda, Mr. Shigeru Kano and all other members of Sato's research group for their helpful and valuable suggestions.

The author has great pleasure to express heartfelt gratitude to my parents, Kenkichi Toda and Takako Toda, for providing a chance to study at Niigata University.